HHS Public Access

Author manuscript

J Comp Neurol. Author manuscript; available in PMC 2017 August 21.

Published in final edited form as:

J Comp Neurol. 2014 June 15; 522(9): 2107–2128. doi:10.1002/cne.23520.

Intense and Specialized Dendritic Localization of the Fragile X Mental Retardation Protein in Binaural Brainstem Neurons -- a Comparative Study in the Alligator, Chicken, Gerbil, and Human

Yuan Wang[1], **Hitomi Sakano**[1], **Karisa Beebe**[2], **Maile R. Brown**[3], **Rian de Laat**[4], **Mark Bothwell**[4], **Randy J. Kulesza Jr.**[2], and **Edwin W Rubel**[1]

[1]Virginia Merrill Bloedel Hearing Research Center, Department of Otolaryngology-Head and Neck Surgery, University of Washington School of Medicine, Seattle, WA 98195-7923, USA

[2]Lake Erie College of Osteopathic Medicine, 1858 West Grandview Boulevard, Erie, PA 16509, USA

[3]Department of Pharmacology, Yale University School of Medicine, 333 Cedar Street, New Haven, CT 06520-8066, USA

[4]Institute for Stem Cell and Regenerative Medicine and Department of Physiology and Biophysics, University of Washington, Seattle, WA 98109, USA

Abstract

Neuronal dendrites are structurally and functionally dynamic in response to changes in afferent activity. The fragile X mental retardation protein (FMRP) is an mRNA binding protein that regulates activity-dependent protein synthesis and morphological dynamics of dendrites. Loss and abnormal expression of FMRP occur in fragile X syndrome (FXS) and some forms of autism spectrum disorders. To provide further understanding of how FMRP signaling regulates dendritic dynamics, we have examined dendritic expression and localization of FMRP in the reptilian and avian nucleus laminaris (NL) and its mammalian analogue, the medial superior olive (MSO), in rodents and humans. NL/MSO neurons are specialized for temporal processing of low frequency sounds for binaural hearing, which is impaired in FXS. Protein BLAST analyses first demonstrate that the FMRP amino acid sequences in the alligator and chicken are highly similar to human FMRP with identical mRNA-binding and phosphorylation sites, suggesting that FMRP functions similarly across vertebrates. Immunocytochemistry further reveals that NL/MSO neurons have very high levels of dendritic FMRP in low frequency hearing vertebrates including alligator, chicken, gerbil, and human. Remarkably, dendritic FMRP in NL/MSO neurons often accumulates at branch points and enlarged distal tips, loci known to be critical for branch-specific dendritic

Correspondence to: Edwin W Rubel, Virginia Merrill Bloedel Hearing Research Center, Mail Stop 357923, University of Washington, Seattle, WA 98195; Phone: (206) 543-8360; Fax: (206) 616-1828; rubel@uw.edu.

Conflict of Interest Statement

The authors have no identified conflict of interest.

Role of Authors

All authors had full access to all the data in the study and take responsibility for the integrity of the data and the accuracy of the data analysis. Study concept and design: Wang Y and Rubel EW. Acquisition of data: Wang Y, Sakano H, Beebe K, Brown MR, Laat R, and Bothwell M. Analysis and interpretation of data: Wang Y, Bothwell M, and Kulesza RJ. Drafting of the manuscript: Wang Y, Bothwell M, and Kulesza RJ. Statistical analysis: Wang Y. Obtained funding: Rubel EW, Bothwell M, and Kulesza RJ.

arbor dynamics. These observations support an important role for FMRP in regulating dendritic properties of binaural neurons that are essential for low frequency sound localization and auditory scene segregation, and support the relevance of studying this regulation in nonhuman vertebrates that use low frequencies in order to further understand human auditory processing disorders.

Keywords

fragile X syndrome; dendritic regulation; nucleus laminaris; medial superior olive; low frequency temporal processing; brain evolution

Introduction

Dendritic morphology and intrinsic properties shape firing patterns of a neuron. Dendritic defects are among the strongest pathological correlates with cognitive disability (Kaufmann and Moser, 2000) and are associated with numerous neurodevelopmental disorders as well as with neurodegeneration (McGlashan and Hoffman, 2000; Kamiya et al., 2005; Burke and Barnes, 2006; Hayashi-Takagi et al., 2010).

Dramatic manifestation of dendritic defects associated with severe behavioral consequences is observed in fragile X syndrome (FXS), the leading known genetic cause of autism spectrum disorder (reviewed in Santoro et al., 2012). FXS patients exhibit intellectual disability as well as sensory and motor dysfunction. FXS is caused by trinucleotide repeat expansions of an X-linked gene, FMR1, which results in the transcriptional silencing and loss of the FMR1 protein product, the fragile X mental retardation protein (FMRP; reviewed in Penagarikano et al., 2007; Bagni et al., 2012). Brains of FXS patients and FMR1 knockout mice show abnormal morphology of dendritic spines (Rudelli et al., 1985; Hinton et al., 1991; Comery et al., 1997; Irwin et al., 2001; 2002; McKinney et al., 2005; Levenga et al., 2011) and dendritic arborizations (Braun and Segal, 2000; Galvez et al., 2003, 2005; Castrén et al., 2005; Restivo et al., 2005; Zarnescu et al., 2005; Thomas et al., 2008; Qin et al., 2011; Scotto-Lomassese et al., 2011; Till et al., 2012).

In the normal brain, FMRP is associated with ribosomes. Its apparent roles are to reversibly suppress translation of specific mRNAs and to release mRNAs for translation upon changes in a variety of conditions, including changes in neural activity (Darnell et al., 2011). Possible roles of FMRP in dendritic spines have been extensively studied in the cortex and have been linked to spine pruning during normal development (Comery et al., 1997; Portera-Cailliau, 2012) and activity-dependent synaptic plasticity via mGluR signaling (Bear et al., 2004; Santoro et al., 2012). Abnormal spine development and reduced synaptic plasticity in FXS brains have been implicated in the intellectual impairments observed in FXS individuals (reviewed in Bear et al., 2004; Santoro et al., 2012). However, relatively little is known about how FMRP regulates global dendritic arborization in vertebrates, and how this regulation relates to the behavioral deficits observed in FXS individuals.”

The binaural circuit specialized for low frequency temporal processing in the auditory brainstem provides a functionally relevant model to address these questions. Across vertebrate species with low frequency hearing, from reptiles and birds to mammals including

humans, the general organization of this circuit is highly conserved (Moore, 2000; Carr and Soares, 2002; Carr et al., 2009; reviewed in Burger and Rubel, 2008; Fig. 1). The nucleus magnocellularis (NM) and nucleus laminaris (NL) in reptiles and birds, the key excitatory nuclei of the binaural circuit, are structurally and functionally similar to the mammalian ventral cochlear nucleus (VCN) and medial superior olive (MSO), respectively. NM/VCN neurons receive temporally locked excitatory signals elicited by low-frequency sounds from the auditory nerve, and in turn, send bilaterally segregated signals to NL/MSO. Dendrites of NL and MSO neurons segregate into two domains; each domain receives excitatory input from the ipsilateral or contralateral NM/VCN. This anatomic segregation, along with specialized synaptic and intrinsic physiology, enable NL/MSO neurons to compute interaural time differences (ITDs), i.e. time disparities in the arrival of signals between the two ears, a critical binaural cue for sound localization and segregation.

Detailed psychophysical and behavioral studies in patients with FXS have identified impaired temporal processing as a specific form of visual and auditory dysfunction and have attributed such impairment to abnormal information processing at both cortical and subcortical levels (Kogan et al., 2004; Hall et al., 2009; Tobia and Woodruff-Pak, 2009; Farzin et al., 2011; Roy et al., 2011). Remarkably, FMRP level is also tightly associated with visual temporal performance among healthy individuals (Kéri and Benedek, 2011). At the cellular level, FMRP is required for proper dynamics of potassium channels and rapid neuronal firing with high temporal accuracy in the auditory brainstem (Brown et al., 2010; Strumbos et al., 2010; reviewed in Brown and Kaczmarek, 2011). In addition, several lines of evidence have established VCN and MSO and their function as prominent targets in autistic patients, although whether these patients specifically have FXS is mostly unknown. These lines of evidence include abnormal organization of the superior olivary complex, in particular the MSO (Kulesza and Mangunay, 2008; Kulesza et al., 2011), delayed cortical responses to low frequency tones (Roberts et al., 2010), and difficulty of detecting speech in noise and localizing sounds (Alcántara et al., 2004, 2012; Teder-Sälejärvi et al., 2005). Thus, a logical hypothesis is that FMRP regulates dendritic structure and intrinsic electrical properties of the brainstem binaural neurons.

To begin to examine this hypothesis and to establish an animal model for basic research, the current study provides genetic and anatomic evidence in support of an important role for FMRP in regulating NL/MSO dendrites and demonstrates the conservation of this regulation across vertebrates. We compare the amino acid sequence of FMRP and its subcellular dendritic localization in NL and MSO neurons across four vertebrate species: alligator, chicken, gerbil, and human. These species are known to have a well-developed NL or MSO, use ITDs as primary binaural cues, and specialize in low frequency hearing (Moore, 2000; Higgs et al., 2002; Seidl and Grothe, 2005; Burger and Rubel, 2008; Carr et al., 2009).

Materials and Methods

Animals

The brainstem tissue from three juvenile American alligator (*Alligator mississippiensis*) was used for immunocytochemistry. These animals were obtained from the Rockefeller Wildlife Refuge (Grand Chenier, LA). One brainstem block was fixed and generously provided by

Drs. Michael B. Pritz (Indiana University), Duncan B. Leitch (Vanderbilt University), and Kenneth C. Catania (Vanderbilt University), while the other two were provided by Dr. Catherine E. Carr (University of Maryland). Snap-frozen tissue from the brainstem of an additional juvenile American alligator, generously provided by Dr. Catherine E. Carr, was used for Western blot.

Seven White Leghorn chicken hatchlings (*Gallus gallus domesticus*; 2–10 days old) of either sex were used for immunocytochemistry (n=5) and Western blot (n=2). Eggs were obtained from Featherland Farms (Eugene, OR) and incubated and hatched at a University of Washington vivarium.

Six female Mongolian gerbils (*Meriones unguiculatus*) were purchased from the Charles River Laboratories (Wilmington, MA, USA). Two adults and two 25-day-old gerbils were used for immunocytochemistry. No difference was detected in the staining pattern in MSO between the two age groups. Two additional 25-day-old gerbils were used for Western blot. In addition, one male albino Sprague-Dawley rat (*Rattus norvegicus*; 6-week-old) was purchased from the Harlan Laboratories (Indiana, IN, USA) and used for Western blot.

All procedures were approved by the University of Washington Institutional Animal Care and Use Committee and carried out in accordance with the National Institutes of Health Guide for the Care and Use of Laboratory Animals.

Human tissues

We investigated MSO in four human brainstems from individuals ranging in age from 57 to 84 years of age (average 75±6.17; 3 female and 1 male). Specimens were obtained from donated cadavers and the IRB granted exempt status for all procedures. These brainstems match the following four criteria: (1) the cause of death was not neurological or metastatic cancer affecting the brainstem, (2) there were no signs of degenerative disease, (3) there were no signs of brainstem pathology, trauma or vascular compromise, and (4) the brainstems were preserved within 24 hours of death.

Antibody characterization

Three primary antibodies were used for Western blot and immunocytochemistry. The optimal primary antibody concentration was obtained by running a series of concentration tests to avoid floor or ceiling truncation, including a negative control by omitting primary antibody. Immunogen, host species, clone type, manufacturer's information, as well as dilution used for each antibody in each species, are listed in Table 1.

Rabbit polyclonal anti-FMRP was raised against synthetic peptide conjugated to KLH derived from within residues 550 to the C-terminal of human FMRP. The amino acid sequence of the exact antigen is highly similar between the alligator, chicken, and human FMRP. The specificity of the antibody is verified by Western blot on a number of rat and human cell lines (manufacturer's data sheet), as well as on mouse brain tissue (Darnell et al., 2011). The antibody specificity is further tested by Western blot in the current study on brain tissues collected from the alligator, chicken, and gerbil, using mouse and rat brain tissue as positive controls (see the Results).

Mouse monoclonal anti-microtubule associated protein 2 (MAP2) detects endogenous levels of MAP2a and MAP2b protein, a neuronal marker that associates with microtubules, neurofilaments, and actin filaments. According to the manufacturer's data sheet, anti-MAP2 recognizes rat, mouse and chicken MAP2 as 200–300 kDa bands on Western blots. This antibody has been used as a somatodendritic marker in the chicken brain (Wang et al., 2009; McBride et al., 2013). The staining pattern in the current study is comparable to that reported in these studies.

Rabbit polyclonal anti-β-actin was used as a loading control in Western blot analysis. The immunogen is synthetic peptide derived from within residues 1–100 of human β-actin. The specificity of the antibody is tested by Western blot on human cells and mouse brain (manufacturer's data sheet) and on alligator, chicken, and gerbil brains in the current study.

Western blot

Protein samples were harvested from the brainstem of the alligator, chicken, and gerbil, as well as from the olfactory bulb of the mouse and the cortex of the rat. All samples were sonicated in Tris buffer (20 mM Tris pH 7.5, 150 mM NaCl, and 2 mM EDTA) with protease inhibitor (Sigma, St. Louis, MO) and centrifuged at 2300 xg for 10 min. The supernatant was collected and sampled for Bradford protein assay (Bio-Rad, Hercules, CA). Each sample (10 μg or 30 μg protein) was diluted in 6× Laemli buffer (300 mM Tris pH 6.8, 600 mM DTT, 12% SDS, 0.6% bromophenol blue, and 60% glycerol), incubated at 65°C for one hour, subjected to SDS-PAGE on 10% gel, and transferred to PVDF membrane. Membranes were incubated in 5% milk in phosphate buffered saline (PBS) with 0.1% Tween for one hour, primary antibody solution (anti-FMRP, 1:2000; anti-β-actin, 1:1000) for 2 hours, and secondary antibody solution (HRP-conjugated donkey-anti-rabbit, 1:200,000; Jackson ImmunoResearch Laboratories, West Grove, PA) with 2% milk for one hour. The blots were then developed with Immobilon chemiluminescent HRP substrate (Millipore, Billerica, MA) and X-ray film. Blots were stripped with Restore buffer (Bio-Rad) between different primary antibody stains.

Immunocytochemistry on nonhuman brainstems

Chickens and gerbils were transcardially perfused with 0.9% saline followed by 4% paraformaldehyde in 0.1 M phosphate buffer (PB). The brains were removed from the skull, post-fixed overnight in the same fixative, and transferred to 30% sucrose in 0.1 M PB with 0.02% sodium azide. For the alligator, following perfusion with 4% paraformaldehyde, the brainstem was blocked, post-fixed, embedded in gelatin, and stored in a mixture of 30% sucrose and 4% paraformaldehyde in 0.01 M PBS.

All brains and brainstem blocks were then sectioned in the coronal plane at 30 μm on a freezing sliding microtome. Each section was collected in PBS with 0.02% sodium azide. Alternate serial sections were stained for Nissl substance or immunocytochemically for FMRP and MAP2 (used as a somatodendritic marker) as described previously (Wang et al., 2009). Briefly, free-floating sections were incubated with primary antibody solutions diluted in PBS with 0.3% Triton X-100 overnight at 4°C, followed by biotinylated anti-IgG antibodies (1:200; Vector Laboratories, Burlingame, CA) or AlexaFluor® secondary

antibodies (1:200; Molecular Probes, Eugene, OR) for 2 hours at room temperature. For peroxidase staining of single antibody, sections were incubated in avidin-biotin-peroxidase complex solution (ABC Elite kit; Vector Laboratories) diluted 1:100 in PBS with 0.3% Triton X-100 for 1 hour at room temperature. Sections were incubated for 3–7 minutes in 0.015% 3-3′-diaminobenzidine (Sigma) with 0.03% hydrogen peroxide, 125 mM sodium acetate, 10 mM imidazole, and 100 mM nickel ammonium sulfate. Sections were mounted on gelatin-coated slides and then dehydrated, cleared, and coverslipped with DPX mounting medium (EMS, Hatfield, PA). For double fluorescent staining, sections were mounted following the secondary antibody incubation and coverslipped with Fluoromount-G® (SouthernBiotech, Birmingham, AL).

Immunocytochemistry on human brainstems

Human brainstems were dissected from the skull within 24 hours of death and post-fixed for at least two weeks in 4% paraformaldehyde in 0.1M PB. Brainstems were then placed in a solution of 30% sucrose and 4% paraformaldehyde in 0.1M PB until they were saturated (about 2 weeks). Brainstems were sectioned in the horizontal plane on a freezing microtome at 40 μm and collected free-floating in PB. Every tissue section was collected beginning from the pontobulbar body and extending rostrally to the exit of the trigeminal nerve. Alternating series of sections were stained for Nissl (Giemsa; Iñiguez et al., 1985; see Kulesza, 2007) or for immunocytochemistry.

For FMRP immunocytochemistry, endogenous peroxidase activity was quenched by 1.5% hydrogen peroxide in PB and cells were permeabilized in 0.5% Triton X-100. Sections were blocked for 45–60 minutes in 1% normal donkey serum and then incubated for at least 20 hours at room temperature with primary antibody solutions diluted in 1% normal donkey serum in PB. Sections were then rinsed and incubated for at least 2 hours in biotinylated secondary antibody (1:100; Vector Laboratories) followed by an incubation in avidin-biotin complex solution for 2 hours. The chromagen reaction was developed in a solution of 0.05% diaminobenzidine and 0.01% hydrogen peroxide with heavy metal intensification (Adams, 1981). Finally, sections were mounted on glass slides, counterstained with Neutral Red, and sealed under coverslips with Permount (Fisher Scientific, Pittsburgh, PA).

Cell filling in fixed sections

Individual NL neurons in the chicken were dye-filled as described previously (Wang and Rubel, 2012). Briefly, 50-μm-thick sections containing NL neurons were prepared from a fixed chicken brainstem. Individual neurons in NL were filled with AlexaFluor® 488 dextran (Invitrogen, Eugene, OR) using electroporation. Fluorescent immunocytochemistry for FMRP was then performed as described above on sections containing dye-filled neurons. Filled neurons and FMRP immunoreactivity were imaged using confocal microscopy (Fluoview 1000; Olympus, Center Valley, PA). Following deconvolution of the image stacks, neuronal morphology and FMRP immunoreactivity were surface rendered and visualized using Huygens Professional software (Scientific Volume Imaging, Hilversum, North Holland, Netherlands).

Quantitative analyses

Two quantitative analyses were conducted in the alligator (n=1), chicken (n=4), and gerbil (n=3). All measurements were made from sections with fluorescent double labeling for FMRP and MAP2 immunoreactivities. The two channels were imaged sequentially using an Olympus FV-1000 confocal microscope to avoid bleed-through between channels.

Regional comparison—This analysis is to compare the level of FMRP staining between the dendritic layers of NL/MSO and the surrounding dendrite-rich regions in the brainstem, the latter referred to as the "reference region" here. This reference region is the adjacent ventral brainstem area in the alligator (see box in Fig. 4A as an example) and chicken (see box c in Fig. 8A) and the brainstem regions just dorsal to the superior olivary complex in the gerbil (see box c in Fig. 12A). In all cases, comparisons were made within the same tissue section to avoid possible inconsistencies caused by variations in immunostaining. MAP2 staining was used in this analysis as an approximate indicator of the density of dendritic branches in a given region.

For each animal, NL or MSO was divided into three portions along its rostrocaudal axis. One section was chosen from each portion. For each section, three areas in the NL/MSO dendritic layers and three addition areas in the reference regions were chosen. Images of both FMRP and MAP2 channels were taken from these six areas at a total magnification of 800×. For each image, the average optical density of labeling was measured for each channel in the ImageJ software (version 1.38X; National Institutes of Health). The ratio of the optical density of FMRP to MAP2 channels was calculated for each area and used as individual data points for comparison between the NL/MSO dendritic layers and the adjacent reference regions using a two-tailed Student's t-test (see Fig. 6A; $p < 0.05$ was considered statistically significant). In addition, the mean of the ratio was calculated across all three areas of the reference region in the same section and used as the standard to which the ratio of the optical density in NL/MSO dendritic layers of the same section was normalized. This calculation is described by the following formula with OD representing optical density:

$$\begin{aligned}&\text{relative FMRP/MAP2 intensity ratio}\\&=(\text{FMRP\_ OD}_{\text{NL}}/\text{MAP2\_ OD}_{\text{NL}})/\text{mean}\,(\text{FMAP\_ OD}_{\text{reference}}/\text{MAP2\_ OD}_{\text{reference}})\end{aligned}$$

Each relative FMRP/MAP2 intensity ratio was used as a single data point and compiled across all imaged NL regions from all animals for each species. A value greater or smaller than 1 means the FMRP/MAP2 ratio in NL/MSO is greater or smaller than that in surrounding areas, and thus indicates a higher or lower concentration of FMRP per dendritic branch in NL/MSO than in the surrounding areas.

FMRP Localization index—The purpose of this analysis is to quantify the degree of FMRP accumulation at branch points and enlarged distal tips relative to FMRP localization along dendritic shafts. MAP2 staining was used to identify individual branch points and enlarged distal tips that are a continuation of a portion of the proximal dendritic shaft within the same tissue section. The total number of samples analyzed was 32–45 for each species, with the sampling sizes for each structure (branch points or enlarged distal tips) indicated in

Fig. 6B–C. For each isolated dendritic structure, the average optical density of FMRP labeling was measured in ImageJ software within a round window placed within the branch point, within the enlarged portion of the distal tips or along the proximal dendritic shaft. The size of the window is 0.5–4.9 μm in diameter, depending on the diameter of the dendritic branch and the size of the branch point or enlarged distal tips. Following the subtraction of the background optical density measured from a dendrite-free region in the same section, these optical intensities were used as individual data points for comparison between the branch points (or enlarged distal tips) and the proximal dendrites of the same branches using a two-tailed Student's t-test ($p < 0.05$ was considered statistically significant). In addition, localization index was calculated as the difference in the optical intensity between a branch point (or enlarged distal tips) and its proximal shaft normalized to the sum of the two intensities. This calculation is described by the following formula with OD representing optical density:

$$\text{localization index} = (\text{OD}_{\text{BP or TE}} - \text{OD}_{\text{shaft}}) / (\text{OD}_{\text{BP or TE}} + \text{OD}_{\text{shaft}})$$

BP and TE in the formula indicate branch point and enlarged distal tips, respectively. The localization index was averaged and graphed using a Box-and-Whisker plot for each structural type and species.

Imaging

Digital images of selected sections were captured with a Zeiss Axioplan microscope and collected in SlideBook (Intelligent Imaging Innovations, Denver, CO) or by using confocal microscopy (Fluoview 1000; Olympus). Image brightness, gamma, and contrast adjustments, as well as photomontages, were performed in Adobe Photoshop (Adobe Systems, Mountain View, CA). All adjustments were applied equally to each entire tissue section.

Results

Comparison of FMRP amino acid sequence

Amino acid sequences of the chicken and human FMRP were obtained from the NCBI-UniGene website (http://www.ncbi.nlm.nih.gov/unigene). The raw sequence file of the alligator (*Alligator mississippiensis*) genome was provided by the International Crocodilian Genomes Working Group (St John et al., 2012; downloaded from ftp://ftp.crocgenomes.org/pub/alligator.current/). The alligator FMRP was first assembled from the alligator genome by BLAST analysis using the chicken FMRP sequence (Gator-a in Fig. 2). Similar to humans, chickens and alligators have two paralogs, FMR1 and FMR2, and three FMR1-like genes, including the FMR1 ortholog and two FXR (fragile X mental retardation syndrome-related protein) genes. Deduced amino acid sequences of FMRP in the alligator and chicken are very similar to the human sequence, except for the lack of sequences corresponding to human FMR1 exons 11 or 12 (magenta line in Fig. 2). The putative phosphorylation sites in human FMRP are completely conserved in alligators and chickens. In addition, the RGG box and KH domains, known mRNA-binding sites of the human FMRP, are nearly identical in alligators and chickens.

To detect potential exons of the alligator FMR1 that are not present in the chicken sequence, we used the Genscan Web Server at the Massachusetts Institute of Technology (MIT) as an additional method to predict the alligator FMRP. Genscan predicts that the alligator FMRP has a long extension at the amino-terminus, and/or a longer sequence in the middle of the protein (Gator-b in Fig. 2). Both possibilities seem reasonable as some human FMRP transcripts include an additional 5′ exon encoding an amino-terminal extension, and a variably spliced exon corresponding to the location where the long additional alligator exon is predicted in different species, based on ESTs (Expressed Sequence Tags) in the Genbank database (http://www.ncbi.nlm.nih.gov/genbank).

Based on the ESTs available, we further compared splice variants between chicken and human FMRP. Similar to the human, deletion of the first part of exon 17 is common in chicken. Both chicken and human FMRPs have splice variants that eliminate the phosphorylation sites in exon 15 and splice variants that incorporate an exon encoding only 4 amino acids followed by a stop codon which produces a protein that is truncated immediately after the first KH domain. Chicken FMRP sometimes lacks exon 4, which is not reported in humans. On the other hand, we have not found a chicken transcript that deletes the nuclear export signal encoded by exon 14, as found in variants detected in humans and mice (Brackett et al., 2013).

Western blot analyses

Western blot immunoassay verifies the specificity of the anti-FMRP antibody used in the current study in the alligator, chicken, gerbil, mouse, and rat. The results shown in Figure 3 illustrate a common band (~ 80 kDa) recognized among mouse, rat, and gerbil, corresponding to the FMRP previously identified in the mouse using the same antibody (Darnell et al., 2011). The rat and gerbil FMRPs show an additional band at a slightly lower molecular weight (~ 70 kDa). A 70-kDa band is the major band recognized in the chicken, probably reflecting the lack of sequence corresponding to the mammalian exons 11 and 12 (of predicted molecular weight: 7.4 kDa). The alligator FMRP exhibits two detectable bands, a weak band at 70 kDa and a strong band at a higher molecular weight (~ 90 kDa). The 90 kDa band may result from the long amino-terminus extension (of predicted molecular weight: 20.0 kDa) or additional exon (of predicted molecular weight: 16.3 kDa) of the alligator FMRP as predicted by Genscan.

In addition to these bands within the predicted molecular weight range, bands around 30 kDa or 180 kDa were also detected, in particular on the mammalian tissues. Some of these extra bands have been reported on human Hela cells and mouse brain (manufacturer’s data sheet), but their identities are unknown.

FMRP immunoreactivity in the alligator NL

As observed in low power image (Fig. 4A), the alligator NM and NL show very high levels of FMRP immunoreactivity, distinct from the majority of other regions in the brainstem. NM and NL contain darkly labeled cell bodies and neuropil regions. In contrast, the more ventrally located brainstem regions contain mostly lightly stained cell bodies and neuropil although these regions are rich in dendrites as indicated by MAP2 staining (Fig. 4B–C).

Within NL, neurons are arranged in a laminar pattern with multiple layers of cell bodies in the caudolateral NL (Fig. 5G) and a single layer of cell bodies in the more rostral and medial portions of the nucleus (Fig. 5H). Dendrites of NL neurons are segregated into dorsal and ventral layers, separated by the cell bodies (Fig. 5A–C). The thickness of the dendritic layers decreases gradually from caudolateral to rostromedial. Within the dendritic layers, the density of MAP2-stained dendritic branches exhibits a clear gradient with the caudolateral NL having more dendritic branches per area than the rostromedial portion of the nucleus. High power images reveal that the caudolateral NL is mostly composed of thin, highly-branched dendrites, while neurons situated more rostrally and medially have less branched dendrites of relatively larger diameters (Fig. 5I–L).

FMRP immunostaining in the alligator NL is intense in both cell bodies and throughout the dendritic layers (Fig. 5D–F). Double labeling of FMRP and MAP2 confirms that each MAP2-stained cell body contains FMRP immunoreactivity and the majority of FMRP immunoreactivity in the dendritic layers overlaps with MAP2-stained dendritic branches. Accompanying the gradient of dendritic branch density, the average intensity of FMRP immunoreactivity decreases from caudolateral to rostromedial. The most caudolateral region of NL is characterized by a very high density of small FMRP puncta (Fig. 5M–N). In more rostral and medial portions of NL, the density of FMRP puncta gradually decreases, while the size of individual FMRP puncta gradually increases (Fig. 5O). In the most rostral tip of the nucleus, FMRP immunoreactivity appears distributed relatively more uniformly along individual dendritic branches (Fig. 5P).

Quantitative analyses indicate that the ratio of optical density between FMRP and MAP2 staining is significantly higher in NL dendritic layers than in the surrounding brainstem regions (Fig. 6A; paired t-test, $p < 0.0001$, n=18). The relative FMRP/MAP2 ratio, calculated as the FMRP/MAP2 ratio in NL dendritic layers divided by the ratio in the surrounding brainstem, is 2.85 ± 0.56 (mean ± S.D., n=9), indicating that the optical intensity of FMRP immunoreactivity in NL dendrites is 2–3 fold higher than in neuronal dendrites of the surrounding brainstem.

High power images reveal substantial FMRP immunoreactivity throughout NL dendritic branches. FMRP immunoreactive particles often form clusters, showing a complementary pattern to that of MAP2 immunoreactivity (Fig. 7). That is, FMRP clusters tend to accumulate within dendritic compartments that have relatively low levels of MAP2. Many of these compartments are branch points (Fig. 7A–E) and enlarged distal tips (Fig. 7F–J) but some are also found to be swellings along the main dendritic shafts. This complementary accumulation pattern of FMRP is less dramatic in the rostral NL, giving rise to a relatively continuous staining pattern of FMRP along dendritic branches (Fig. 5F and 5P).

The average optical intensity of FMRP labeling at a branch point or enlarged distal tips is significantly higher than in its proximal dendritic shaft (Fig. 6B–C; paired t-test; for branch points: $p < 0.0001$, n=17; for enlarged distal tips: $p < 0.0001$, n=16). To further evaluate this accumulation pattern, we calculated the localization index, i.e., normalized FMRP intensity at a branch point or enlarged distal tips relative to that in its proximal dendritic shaft (Fig. 6D). A positive index indicates a stronger localization of FMRP staining at a branch point or

enlarged distal tip than the main shaft. The maximal value of an index is 1 when no FMRP proteins present in main dendritic shafts. Among all sampled dendritic structures, 88% branch points (15 in 17) and 100% enlarged distal tips (16 in 16) have a positive localization index. The average mean localization index across all samples is 0.45 ± 0.34 (mean ± S.D., n=17) for branch points and 0.65 ± 0.23 (mean ± S.D., n=16) for enlarged distal tips.

FMRP immunoreactivity in the chicken NL

The organization of the chicken NL is similar to the alligator, a three-layer configuration with two dendritic layers separated by a single cell layer of somata (Smith and Rubel, 1979; Wang and Rubel, 2008; Fig. 8A–B). NL neurons in chickens exhibit intense FMRP immunoreactivity in the cytoplasm and throughout the dorsal and ventral dendritic layers (Fig. 8D–E). Again, a much higher intensity of FMRP labeling in NL dendritic layers than other dendrite-rich regions in the ventral brainstem is observed (Fig. 8C–F) and quantitatively confirmed (Fig. 6A; paired t-test, $p < 0.0001$, n=18). The relative FMRP/MAP2 ratio in the chicken NL is 1.99 ± 0.52 (mean ± S.D., n=9), indicating an on average 2 folds dendritic FMRP density in NL when compared to the surrounding ventral brainstem. No substantial immunoreactivity for FMRP is detected in the immediate adjacent regions of NL that are rich in glial cells and axons (stars in Fig. 8D).

Although NL exhibits a gradient of dendritic extension from the soma along the caudorostral axis in both the chicken and alligator, in contrast to alligator, the chicken NL does not vary significantly in the average density or the diameter of dendritic branches along the axis (Fig. 9A, 9D, 9G). Consistently, the distribution pattern and the average intensity of dendritic FMRP immunostaining in the chicken NL are comparable throughout the nucleus (Fig. 9B, 9E, 9H). Double labeling of FMRP and MAP2 confirms that the majority of FMRP immunoreactivity overlaps with MAP2-stained dendritic branches (Fig. 9C, 9F, 9I, 10). The complementary pattern of FMRP and MAP2 within dendritic compartments is more dramatic in the chicken than in the alligator. Throughout the chicken NL, dendritic FMRP clusters are consistently localized within or very close to branch points (Fig. 10A–E) and enlarged distal tips (Fig. 10F–J). The average optical intensity of FMRP labeling at a branch point or enlarged distal tip is significantly higher than in its proximal dendritic shaft (Fig. 6B–C; paired t-test; for branch points: $p < 0.0001$, n=24; for enlarged distal tips: $p < 0.0001$, n=21). Among all quantified dendritic structures, 100% branch points (24 in 24) and 95% enlarged distal tips (20 in 21) have a positive localization index (Fig. 6D). The average localization index across all samples is 0.50 ± 0.25 (mean ± S.D., n=24) for branch points and 0.63 ± 0.31(mean ± S.D., n=21) for enlarged distal tips. Again, MAP2 level in these FMRP cluster-containing compartments is usually low compared to other portions of the same dendritic branches.

To better visualize the localization pattern of FMRP in NL dendrites, we mapped FMRP immunoreactivity on individual NL neurons filled with a fluorescent dye (Fig. 11). Although FMRP immunoreactivity is detected throughout dye-filled dendritic branches, the majority of FMRP immunoreactivity is distributed within or very close to enlarged distal tips and branch points. In addition, the majority of filled branch points and enlarged distal tips contain intense FMRP clusters.

FMRP immunoreactivity in the gerbil MSO

Unlike most other rodents, gerbils are specialized for low frequency hearing and have a well-developed MSO. The gerbil MSO is situated in the ventral brainstem, surrounded by other auditory nuclei of the superior olivary complex (SOC; Fig. 12A). Similar to the alligator and chicken NL, the gerbil MSO exhibits a three-layer architecture with the lateral and medial dendritic layers separated by the cell body layer (Fig. 12B). In low power images, the average intensity of FMRP immunoreactivity is notably higher in MSO and other SOC nuclei than in surrounding brainstem regions situated more dorsally (Fig. 12D). Closer views reveal a higher intensity of FMRP immunoreactivity within the dendritic layers of MSO than in the dorsal brainstem, which has a high density of MAP2-stained dendritic branches (Fig. 12B–C and 12E–F). Quantitative analyses again confirm that the FMRP/MAP2 ratio in MSO dendritic layers is significantly higher than that in the brainstem regions of the same section, but outside the auditory pathways (Fig. 6A; paired t-test, $p < 0.0001$, n=18). The relative FMRP/MAP2 ratio is 2.51 ± 0.55 (mean ± S.D., n=18). The vast majority of MSO neurons contain strong somatic staining, although occasionally some unstained neurons are seen.

Within the MSO dendritic layers, FMRP immunoreactivity overlaps with MAP2-stained dendritic branches (Fig. 13). Since the dendritic arborization of individual MSO neurons in gerbils is larger than and not as flat as in chicken NL neurons, branch points and enlarged distal tips are less frequently captured on single coronal sections. It is important to note that, similar to the alligator and chicken NL, FMRP immunoreactivity in the gerbil MSO is detected throughout dendritic branches. In some branches, FMRP immunoreactivity exhibits a relatively uniform distribution with comparable intensities in branch points (or distal endings) and dendritic shafts (Fig. 13D–F). However, it is also clear that FMRP is usually not uniformly distributed along dendritic branches. Branch points and enlarged distal tips, identified on the basis of MAP2 immunoreactivity, often display disproportionally intense labeling for FMRP protein (Fig. 13A–C). Quantitatively, the average optical intensity of FMRP labeling at a branch point or enlarged distal tip is significantly higher than in its proximal dendritic shaft across all sampled branches (Fig. 6B–C; paired t-test; for branch points: $p = 0.03$, n=16; for enlarged distal tips: $p = 0.009$, n=16). Among all samples, 75% branch points (12 in 16) and 88% enlarged distal tips (14 in 16) show an accumulation of FMRP as indicated by a positive localization index (Fig. 6D). The average localization index across all samples is 0.20 ± 0.24 (mean ± S.D., n=16) for branch points and 0.34 ± 0.35 (mean ± S.D., n=16) for enlarged distal tips.

An observed difference in our preparations between the gerbil MSO and the alligator and chicken NL is that MAP2 staining in gerbil is relatively uniform along dendritic branches. Thus, the complementary pattern of FMRP and MAP2 immunoreactivities found in the alligator and chicken NL is not as clearly evident in the gerbil MSO.

FMRP immunoreactivity in the human MSO

The MSO is the largest, most conspicuous and most densely populated nucleus within the human SOC. As the chicken NL and the gerbil MSO, the human MSO exhibits a clear three-layer architecture in horizontal sections, consisting of a centrally located column of mostly

fusiform and stellate somata which give rise to both medially and laterally situated dendritic fields. The vast majority of human MSO neurons are FMRP immunoreactive (Fig. 14). However, some FMRP negative somata appear randomly arranged within the nucleus and encompass all morphologies (fusiform, stellate and round). The average intensity of FMRP immunoreactivity in the dendritic layers is much higher compared to the surrounding regions of the brainstem. Due to technical difficulties, we did not successfully visualize human MSO dendrites with MAP2 immunocytochemistry. However, high power images demonstrate that FMRP immunoreactivity is distributed along individual dendritic branches including primary dendrites and higher-order dendritic profiles on either side of the MSO cell layers.

Discussion

In this study, we demonstrate: 1) high protein levels of FMRP in neuronal dendrites of binaural brainstem neurons in the alligator, chicken, gerbil, and human brains; and 2) non-uniform distribution of FMRP along dendritic branches with frequent accumulation at dendritic branch points and enlarged distal tips of these neurons in alligator, chicken, and gerbil. The significance of this intense and specialized localization of dendritic FMRP, as well as the conservation of this localization pattern across low frequency hearing vertebrate species, is discussed below. We relate these findings to the implications for dendritic structural regulation and potential implication in the pathology of fragile X syndrome (FXS) and some forms of autistic spectrum disorders.

High levels of dendritic FMRP in NL and MSO neurons

We found substantial somatic labeling of FMRP in neurons throughout the brainstem, consistent with a previous observation in rats (Feng et al., 1997). The intensity of somatic FMRP immunoreactivity in NL and MSO is notably higher in the alligator and human, but appears similar in the chicken and gerbil, when compared to adjacent brainstem neurons of the same species. Importantly, in all four species, we identified a much higher level of *dendritic* FMRP in NL and MSO neurons as compared to other brainstem regions rich in dendrites. Although FMRP localization has been detected in presynaptic axons (Price et al., 2006; Murashov et al., 2007; Christie et al., 2009) and glial cells (Jacobs et al., 2012) in other brain regions, FMRP level appears low in these cellular components within the dendritic layers of NL and MSO.

Interruption of FMRP signaling may have a great impact on cellular activities occurring within dendrites and thus impair the normal function of neurons. The high FMRP levels in NL and MSO dendrites suggest that they are prominent cellular targets of FMRP-mediated translational regulation in the brainstem. Since NL and MSO dendrites are highly specialized in their structure and physiology for optimizing temporal processing and ITD computation (reviewed in Carr and Soares, 2002; Burger and Rubel, 2008; Wang et al., 2011), interruption of FMRP signaling in NL and MSO dendrites is expected to lead to a significant reduction in the performance and accuracy of these types of processing. This expectation is consistent with recent reports that FMRP level may be used as an index of vulnerability of specific brain regions to the loss of FMRP (Kogan et al., 2004a; Zangenehpour et al., 2009) and is consistent with the positive correlations of FMRP level

with the integrity of neural anatomy (Gothelf et al., 2008), the level of brain activities (Kwon et al., 2001; Hoeft et al., 2007), and the performance of mediated behaviors (Gothelf et al., 2008; Kéri and Benedek, 2009, 2011) in other brain regions that are normally rich in FMRP.

The absolute ability of localizing a sound source or listening in noise has not been carefully studied in patients with FXS or other forms of autism to our knowledge. However, impaired temporal processing has been identified as a common consequence of FMRP loss in visual, auditory, and motor systems (Kogan et al., 2004a, b; Hall et al., 2009; Tobia and Woodruff-Pak, 2009; Farzin et al., 2011; Roy et al., 2011). In addition, two lines of studies have demonstrated significant effects of FMRP loss on auditory temporal processing at the brainstem level. First, significantly greater brain activation in the brainstem (as well as other brain regions) was detected by functional MRI in patients with FXS while performing auditory temporal discrimination tasks when compared to age-matched controls (Hall et al., 2009). Second, in FMR1 knockout mice, neurons in the medial nucleus of the trapezoid body (a SOC nucleus in the auditory brainstem) lost their ability to dynamically regulate ion channels in response to changes in afferent activity and the ability to fire with high temporal accuracy (reviewed in Brown and Kaczmarek, 2011). It is noted that auditory brainstem responses, synchronized auditory evoked potentials from the auditory nerve and brainstem, appear normal in the absence of FMRP (Wisniewski et al., 1985; Miezejeski et al., 1997; Roberts et al., 2005; but also see Ferri et al., 1989; Arinami et al., 1988). One possible interpretation is that FMRP loss-induced changes are restricted to selected cell groups or on specific cellular activities of auditory brainstem neurons, and thus are not measurable by recording of auditory brainstem responses.

Specialized accumulation pattern of dendritic FMRP

FMRP staining in NL and MSO dendrites exhibits a granular or punctate pattern, consistent with observations in hippocampal neurons (Castrén et al., 2001; Antar et al., 2004, 2006) and non-neuronal cells (Castrén et al., 2001; Schrier et al., 2004). In cultured hippocampal neurons, FMRP granules are localized throughout the dendrites, into most spines, and frequently clustered beneath synapses, which gives a relatively uniform distribution of FMRP granules along dendritic branches (Antar et al., 2004, 2006). In addition, the presence of clusters of FMRP granules in dendritic branch points was reported in the adult rat cortex (Feng et al., 1997).

The strong accumulation pattern of FMRP at branch points and enlarged distal tips of NL and MSO dendrites, however, more closely resembles the localization pattern found in developing neurites of other types of neurons. High concentrations of FMRP were found in existing or potential branch points (De Diego Otero et al., 2002; Ferrari et al., 2007), as well as in growth cones of developing neurites (Antar et al., 2006; Hengst et al., 2006). Interestingly, NL and MSO dendrites are also structurally similar to developing neurites. Instead of tapering towards the tip commonly seen in most mature neuronal types, dendritic terminations of NL neurons are characterized by an enlarged bulge, which is often attached with narrow filopodial-like extensions. This structural specialization is prevalent in chicken NL neurons after they have acquired their mature morphology (Deitch and Rubel, 1984; Wang and Rubel, 2012; also see Fig. 11–12 in the current study) and juvenile alligators (see

Fig. 7 in the current study), and sometimes observed in adult gerbils (see Fig. 13 in the current study).

These similarities suggest that FMRP may be strongly involved in structural dynamics of dendritic arbors of NL and MSO neurons. In chickens and gerbils, dendritic arbors undergo dramatic and rapid reorganization in response to changes in afferent input (Deitch and Rubel, 1984; Russell and Moore, 1999; Sorensen and Rubel, 2006, 2011; Wang and Rubel, 2012). Further studies in the chicken found that this reorganization involves selected branch addition and elimination, implicating the involvement of branch-specific mechanisms (Sorensen and Rubel, 2006; Wang and Rubel, 2012). One model that is consistent with this specificity and rapidity is fast switches between enlarged distal tips and branch points (see Discussion in Wang and Rubel, 2012). That is, an ending may quickly turn into a branch point by elongating one of its filopodial-like extensions into a branch. Similarly, a branch point becomes an ending if its daughter branches retract into narrow extensions or completely disappear.

The clustering pattern of FMRP in NL/MSO dendrites gives rise to an intriguing possibility that FMRP plays an important role in determining the fate of individual branches either branching out, retracting, or staying unchanged, and/or provides quick supplies of required proteins for such cellular events on an individual branch basis. A strong support of this possibility comes from a study in neurotrophin-stimulated neurites of PC12 cells (De Diego Otero et al., 2002). High concentrations of endogenous or EGFP-tagged FMRP granules are predominantly localized to swellings along the neurite and in the growth cone, remarkably similar to what we see in NL and MSO dendrites. Importantly, these swellings along the neurite are often locations where new branches are generated. It is interesting to note that abnormal branch length and/or branching pattern of neuronal dendrites in FMR1 knockout or knockin mice are sometimes restricted to arbors of specific orders or locations (Galvez et al., 2003; Thomas et al., 2008; Qin et al., 2011; Till et al., 2012), indicating a differential influence of FMRP in different branches of the same neurons and supporting the involvement of FMRP in branch-specific regulatable mechanisms underlying dendritic branching.

The observation of frequent FMRP accumulation at branch points and enlarged distal tips should not be taken to underestimate potential function of substantial FMRP localization along the dendritic shaft. In addition, single molecules or small granules of FMRP protein may not be visualized by conventional immunocytochemistry at the light microscopy level. It is possible that FMRP proteins synthesized in the cell body are transported to dendrites as single molecules and form puncta or clusters at dendritic swellings as well as branch points and enlarged distal tips for specialized functions or for storage. This possibility is supported by the observation that FMRP distribution can be switched between a diffuse pattern to a granular distribution under certain conditions such as oxidative stress (Dolzhanskaya et al., 2006). Methods that allow sensitive detection of single endogenous FMRP molecules with a high resolution such as *in situ* proximity ligation assay (Jarvius et al., 2007; Liu et al., 2011; Weibrecht et al., 2013) are required to further clarify the localization of FMRP in NL/MSO dendrites.

Chicken NL as a suitable animal model for studying FMRP function

The unusually high expression of FMRP in NL/MSO dendrites in the alligator, chicken, gerbil, and human suggests that this protein is particularly important for highly localized, dynamic regulation of structural and functional properties in these neurons, and that this process is highly conserved along with their bipolar dendritic structure across vertebrate taxa. Although we were not yet able to assess the precise localization of FMRP with the same degree of spatial precision in humans, the accumulation pattern of dendritic FMRP in the dendritic bifurcations and dendritic endings in animal models further suggests that FMRP function involves common cellular mechanisms in both nonmammals and mammals. Characterization of FMRP signaling in this system may have great potential to uncover critical functions of FMRP in the vertebrate brain and help to identify cellular and molecular properties common to the pathologies of fragile X syndrome.

Among these low frequency hearing vertebrates, the chicken circuitry provides an advantageous experimental model for basic research. *First*, it is well documented that the organization and function of the chicken NM/NL circuit are analogous to the VCN/MSO circuit in mammals with low frequency hearing and human (Moore, 2000; Carr and Soares, 2002; Burger and Rubel, 2008). *Second*, chickens have been extensively used in studying binaural hearing and temporal processing. A huge foundation of quantitative data on the structure and physiological properties of developing and mature NM and NL neurons is available (e.g., Rubel and Parks, 1975; Smith, 1981; Jhaveri and Morest, 1982; Funabiki et al., 1998; Kuba et al., 2005; Burger et al., 2005; Gao and Lu, 2008; Blackmer et al., 2009; Sanchez et al., 2010; 2012), providing an enormous advantage for designing experiments and interpreting results. *Third*, the homogeneity and simplicity of the chicken NM and NL enable easy manipulation of afferent input and sensitive assessment of changes in dendritic structure and properties (e.g., Wang and Rubel, 2012). Importantly, dendritic structure of chicken NL, rat and gerbil MSO neurons is regulated by afferent inputs in a comparable, domain-specific pattern (Feng and Rogowski, 1980; Deitch and Rubel, 1984; Russell and Moore, 1999). *Fourth*, the ability to manipulate gene expression with temporal control in individual regions of the chicken brainstem *in vivo* has been developed recently (Schecterson et al., 2012), which allows in-depth exploration of the location and timing of FMRP regulation. *Finally*, a number of identified or predicted FMRP targets, including the plasma membrane calcium ATPase 2, MAP2, and high voltage-activated potassium channel Kv3.1b, have been studied in the chicken NL with documented function in maintaining fundamental structure or optimizing specialized physiological properties, providing promising candidates for characterizing FMRP signaling in relationship to specific neuronal function (Lu et al., 2004; Wang and Rubel, 2008; Wang et al., 2009; Strumbos et al., 2010; Darnell et al., 2011).

Although not as well studied as the chicken NL, the alligator NL provides an interesting model to study the relationship between FMRP expression, dendritic organization, and hearing. As discovered in the current study for the first time, the alligator NL exhibits outstanding high expression of FMRP and dramatic dendritic gradients of multiple structural properties along the tonotopic axis of the nucleus. A recent study has nicely demonstrated that the alligator NL adopts similar physiological strategies for ITD detection as birds (Carr

et al., 2009). As the gradient of dendritic length in the chicken NL is thought to have important functional significance in optimizing ITD computation at particular sound frequencies (Smith and Rubel, 1979; Kuba et al., 2005), it is interesting to explore whether the more dramatic dendritic gradient in the alligator NL is associated with the larger range of best ITD represented in the alligator NL and excellent hearing ability of alligators in both air and water (Higgs et al., 2002; Carr et al., 2009; Vergne et al., 2009). In addition, the relatively high level of somatic FMRP expression in alligator NL and human MSO may implicate a common and particular requirement of FMRP in binaural processing of these two species.

Acknowledgments

Support: National Institute on Deafness and Other Communication Disorders grants DC-011594, DC-03829, DC-02739, DC-04661, and DC-00018; the Lake Erie College of Osteopathic Medicine (LECOM) and Lake Erie Consortium for Osteopathic Medical Training (LECOMT).

We thank Dr. David Morris (University of Washington) for valuable discussion and comments on the manuscript, Drs. Michael B. Pritz (Indiana University), Duncan B. Leitch (Vanderbilt University), Kenneth C. Catania (Vanderbilt University), and Catherine E. Carr (University of Maryland) for alligator brainstem tissue, Dr. Stephanie Furrer (University of Washington) for comments on the manuscript.

Literature Cited

Alcántara JI, Weisblatt EJ, Moore BC, Bolton PF. Speech-in-noise perception in high-functioning individuals with autism or Asperger's syndrome. J Child Psychol Psychiatry. 2004; 45:1107–1114. [PubMed: 15257667]

Antar LN, Afroz R, Dictenberg JB, Carroll RC, Bassell GJ. Metabotropic glutamate receptor activation regulates fragile x mental retardation protein and FMR1 mRNA localization differentially in dendrites and at synapses. J Neurosci. 2004; 24:2648–2655. [PubMed: 15028757]

Antar LN, Li C, Zhang H, Carroll RC, Bassell GJ. Local functions for FMRP in axon growth cone motility and activity-dependent regulation of filopodia and spine synapses. Mol Cell Neurosci. 2006; 32:37–48. [PubMed: 16631377]

Arinami T, Sato M, Nakajima S, Kondo I. Auditory brain-stem responses in the fragile X syndrome. Am J Hum Genet. 1988; 43:46–51. [PubMed: 3376943]

Ashida G, Carr CE. Sound localization: Jeffress and beyond. Curr Opin Neurobiol. 2011; 21:745–751. [PubMed: 21646012]

Bagni C, Tassone F, Neri G, Hagerman R. Fragile X syndrome: causes, diagnosis, mechanisms, and therapeutics. J Clin Invest. 2012; 122:4314–4322. [PubMed: 23202739]

Bear MF, Huber KM, Warren ST. The mGluR theory of fragile X mental retardation. Trends Neurosci. 2004; 27:370–377. [PubMed: 15219735]

Blackmer T, Kuo SP, Bender KJ, Apostolides PF, Trussell LO. Dendritic calcium channels and their activation by synaptic signals in auditory coincidence detector neurons. J Neurophysiol. 2009; 102:1218–1226. [PubMed: 19553482]

Brackett DM, Qing F, Amieux PS, Sellers DL, Horner PJ, Morris DR. FMR1 transcript isoforms: association with polyribosomes; regional and developmental expression in mouse brain. PLoS One. 2013; 8:e58296. [PubMed: 23505481]

Braun K, Segal M. FMRP involvement in formation of synapses among cultured hippocampal neurons. Cereb Cortex. 2000; 10:1045–1052. [PubMed: 11007555]

Brown MR, Kaczmarek LK. Potassium channel modulation and auditory processing. Hear Res. 2011; 279:32–42. [PubMed: 21414395]

Brown MR, Kronengold J, Gazula VR, Chen Y, Strumbos JG, Sigworth FJ, Navaratnam D, Kaczmarek LK. Fragile X mental retardation protein controls gating of the sodium-activated potassium channel Slack. Nat Neurosci. 2010; 13:819–821. [PubMed: 20512134]

Burger RM, Pfeiffer JD, Westrum LE, Bernard A, Rubel EW. Expression of GABA(B) receptor in the avian auditory brainstem: ontogeny, afferent deprivation, and ultrastructure. J Comp Neurol. 2005; 489:11–22. [PubMed: 15977167]

Burger, RM., Rubel, EW. Encoding of interaural timing for binaural hearing. In: Dallos, P., Oertel, D., editors. The senses: a comprehensive reference. San Diego: Academic Press; 2008. p. 613-630.

Burke SN, Barnes CA. Neural plasticity in the ageing brain. Nat Rev Neurosci. 2006; 7:30–40. [PubMed: 16371948]

Carr CE, Soares D. Evolutionary convergence and shared computational principles in the auditory system. Brain Behav Evol. 2002; 59:294–311. [PubMed: 12207085]

Carr CE, Soares D, Smolders J, Simon JZ. Detection of interaural time differences in the alligator. J Neurosci. 2009; 29:7978–7990. [PubMed: 19553438]

Castrén M, Haapasalo A, Oostra BA, Castrén E. Subcellular localization of fragile X mental retardation protein with the I304N mutation in the RNA-binding domain in cultured hippocampal neurons. Cell Mol Neurobiol. 2001; 21:29–38. [PubMed: 11440196]

Castrén M, Tervonen T, Kärkkäinen V, Heinonen S, Castrén E, Larsson K, Bakker CE, Oostra BA, Akerman K. Altered differentiation of neural stem cells in fragile X syndrome. Proc Natl Acad Sci U S A. 2005; 102:17834–17839. [PubMed: 16314562]

Christie SB, Akins MR, Schwob JE, Fallon JR. The FXG: a presynaptic fragile X granule expressed in a subset of developing brain circuits. J Neurosci. 2009; 29:1514–1524. [PubMed: 19193898]

Comery TA, Harris JB, Willems PJ, Oostra BA, Irwin SA, Weiler IJ, Greenough WT. Abnormal dendritic spines in fragile X knockout mice: maturation and pruning deficits. Proc Natl Acad Sci U S A. 1997; 94:5401–5404. [PubMed: 9144249]

Darnell JC, Van Driesche SJ, Zhang C, Hung KY, Mele A, Fraser CE, Stone EF, Chen C, Fak JJ, Chi SW, Licatalosi DD, Richter JD, Darnell RB. FMRP stalls ribosomal translocation on mRNAs linked to synaptic function and autism. Cell. 2011; 146:247–261. [PubMed: 21784246]

Deitch JS, Rubel EW. Afferent influences on brain stem auditory nuclei of the chicken: time course and specificity of dendritic atrophy following deafferentation. J Comp Neurol. 1984; 229:66–79. [PubMed: 6490976]

De Diego Otero Y, Severijnen LA, van Cappellen G, Schrier M, Oostra B, Willemsen R. Transport of fragile X mental retardation protein via granules in neurites of PC12 cells. Mol Cell Biol. 2002; 22:8332–8341. [PubMed: 12417734]

Dolzhanskaya N, Merz G, Denman RB. Oxidative stress reveals heterogeneity of FMRP granules in PC12 cell neurites. Brain Res. 2006; 1112:56–64. [PubMed: 16919243]

Farzin F, Rivera SM, Whitney D. Resolution of spatial and temporal visual attention in infants with fragile X syndrome. Brain. 2011; 134:3355–3368. [PubMed: 22075522]

Feng AS, Rogowski BA. Effects of monaural and binaural occlusion on the morphology of neurons in the medial superior olivary nucleus of the rat. Brain Res. 1980; 189:530–534. [PubMed: 7370789]

Feng Y, Gutekunst CA, Eberhart DE, Yi H, Warren ST, Hersch SM. Fragile X mental retardation protein: nucleocytoplasmic shuttling and association with somatodendritic ribosomes. J Neurosci. 1997; 17:1539–1547. [PubMed: 9030614]

Ferrari F, Mercaldo V, Piccoli G, Sala C, Cannata S, Achsel T, Bagni C. The fragile X mental retardation protein-RNP granules show an mGluR-dependent localization in the post-synaptic spines. Mol Cell Neurosci. 2007; 34:343–354. [PubMed: 17254795]

Ferri. Brain-stem auditory evoked potentials in the fragile X syndrome. Am J Hum Genet. 1989; 45:977–978. [PubMed: 2589325]

Funabiki K, Koyano K, Ohmori H. The role of GABAergic inputs for coincidence detection in the neurones of nucleus laminaris of the chick. J Physiol. 1998; 508(Pt 3):851–869. [PubMed: 9518738]

Galvez R, Gopal AR, Greenough WT. Somatosensory cortical barrel dendritic abnormalities in a mouse model of the fragile X mental retardation syndrome. Brain Res. 2003; 971:83–89. [PubMed: 12691840]

Galvez R, Smith RL, Greenough WT. Olfactory bulb mitral cell dendritic pruning abnormalities in a mouse model of the Fragile-X mental retardation syndrome: further support for FMRP's

involvement in dendritic development. Brain Res Dev Brain Res. 2005; 157:214–216. [PubMed: 15878626]

Gao H, Lu Y. Early development of intrinsic and synaptic properties of chicken nucleus laminaris neurons. Neuroscience. 2008; 153:131–143. [PubMed: 18355968]

Gothelf D, Furfaro JA, Hoeft F, Eckert MA, Hall SS, O'Hara R, Erba HW, Ringel J, Hayashi KM, Patnaik S, Golianu B, Kraemer HC, Thompson PM, Piven J, Reiss AL. Neuroanatomy of fragile X syndrome is associated with aberrant behavior and the fragile X mental retardation protein (FMRP). Ann Neurol. 2008; 63:40–51. [PubMed: 17932962]

Hall SS, Walter E, Sherman E, Hoeft F, Reiss AL. The neural basis of auditory temporal discrimination in girls with fragile X syndrome. J Neurodev Disord. 2009; 1:91–99. [PubMed: 19890439]

Hayashi-Takagi A, Takaki M, Graziane N, Seshadri S, Murdoch H, Dunlop AJ, Makino Y, Seshadri AJ, Ishizuka K, Srivastava DP, Xie Z, Baraban JM, Houslay MD, Tomoda T, Brandon NJ, Kamiya A, Yan Z, Penzes P, Sawa A. Disrupted-in-Schizophrenia 1 (DISC1) regulates spines of the glutamate synapse via Rac1. Nat Neurosci. 2010; 13:327–332. [PubMed: 20139976]

Hengst U, Cox LJ, Macosko EZ, Jaffrey SR. Functional and selective RNA interference in developing axons and growth cones. J Neurosci. 2006; 26:5727–5732. [PubMed: 16723529]

Higgs DM, Brittan-Powell EF, Soares D, Souza MJ, Carr CE, Dooling RJ, Popper AN. Amphibious auditory responses of the American alligator (Alligator mississipiensis). J Comp Physiol A Neuroethol Sens Neural Behav Physiol. 2002; 188:217–223. [PubMed: 11976890]

Hinton VJ, Brown WT, Wisniewski K, Rudelli RD. Analysis of neocortex in three males with the fragile X syndrome. Am J Med Genet. 1991; 41:289–294. [PubMed: 1724112]

Hoeft F, Hernandez A, Parthasarathy S, Watson CL, Hall SS, Reiss AL. Fronto-striatal dysfunction and potential compensatory mechanisms in male adolescents with fragile X syndrome. Hum Brain Mapp. 2007; 28:543–554. [PubMed: 17437282]

Iñiguez C, Gayoso MJ, Carreres J. A versatile and simple method for staining nervous tissue using Giemsa dye. J Neurosci Methods. 1985; 13:77–86. [PubMed: 3887046]

Irwin SA, Idupulapati M, Gilbert ME, Harris JB, Chakravarti AB, Rogers EJ, Crisostomo RA, Larsen BP, Mehta A, Alcantara CJ, Patel B, Swain RA, Weiler IJ, Oostra BA, Greenough WT. Dendritic spine and dendritic field characteristics of layer V pyramidal neurons in the visual cortex of fragile-X knockout mice. Am J Med Genet. 2002; 111:140–146. [PubMed: 12210340]

Irwin SA, Patel B, Idupulapati M, Harris JB, Crisostomo RA, Larsen BP, Kooy F, Willems PJ, Cras P, Kozlowski PB, Swain RA, Weiler IJ, Greenough WT. Abnormal dendritic spine characteristics in the temporal and visual cortices of patients with fragile-X syndrome: a quantitative examination. Am J Med Genet. 2001; 98:161–167. [PubMed: 11223852]

Jacobs S, Cheng C, Doering LC. Probing astrocyte function in fragile X syndrome. Results Probl Cell Differ. 2012; 54:15–31. [PubMed: 22009345]

Jarvius M, Paulsson J, Weibrecht I, Leuchowius KJ, Andersson AC, Wählby C, Gullberg M, Botling J, Sjöblom T, Markova B, Ostman A, Landegren U, Söderberg O. In situ detection of phosphorylated platelet-derived growth factor receptor beta using a generalized proximity ligation method. Mol Cell Proteomics. 2007; 6:1500–1509. [PubMed: 17565975]

Jhaveri S, Morest DK. Neuronal architecture in nucleus magnocellularis of the chicken auditory system with observations on nucleus laminaris: a light and electron microscope study. Neuroscience. 1982; 7:809–836. [PubMed: 7099420]

Kamiya A, Kubo K, Tomoda T, Takaki M, Youn R, Ozeki Y, Sawamura N, Park U, Kudo C, Okawa M, Ross CA, Hatten ME, Nakajima K, Sawa A. A schizophrenia-associated mutation of DISC1 perturbs cerebral cortex development. Nat Cell Biol. 2005; 7:1167–1178. [PubMed: 16299498]

Kaufmann WE, Moser HW. Dendritic anomalies in disorders associated with mental retardation. Cereb Cortex. 2000; 10:981–991. [PubMed: 11007549]

Kéri S, Benedek G. Visual pathway deficit in female fragile X premutation carriers: a potential endophenotype. Brain Cogn. 2009; 69:291–295. [PubMed: 18789568]

Kéri S, Benedek G. Fragile X protein expression is linked to visual functions in healthy male volunteers. Neuroscience. 2011; 192:345–350. [PubMed: 21749915]

Kogan CS, Bertone A, Cornish K, Boutet I, Der Kaloustian VM, Andermann E, Faubert J, Chaudhuri A. Integrative cortical dysfunction and pervasive motion perception deficit in fragile X syndrome. Neurology. 2004a; 63:1634–1639. [PubMed: 15534248]

Kogan CS, Boutet I, Cornish K, Zangenehpour S, Mullen KT, Holden JJ, Der Kaloustian VM, Andermann E, Chaudhuri A. Differential impact of the FMR1 gene on visual processing in fragile X syndrome. Brain. 2004b; 127:591–601. [PubMed: 14736752]

Kuba H, Yamada R, Fukui I, Ohmori H. Tonotopic specialization of auditory coincidence detection in nucleus laminaris of the chick. J Neurosci. 2005; 25:1924–1934. [PubMed: 15728832]

Kulesza RJ. Cytoarchitecture of the human superior olivary complex: medial and lateral superior olive. Hear Res. 2007; 225:80–90. [PubMed: 17250984]

Kulesza RJ, Lukose R, Stevens LV. Malformation of the human superior olive in autistic spectrum disorders. Brain Res. 2011; 1367:360–371. [PubMed: 20946889]

Kulesza RJ, Mangunay K. Morphological features of the medial superior olive in autism. Brain Res. 2008; 1200:132–137. [PubMed: 18291353]

Kwon H, Menon V, Eliez S, Warsofsky IS, White CD, Dyer-Friedman J, Taylor AK, Glover GH, Reiss AL. Functional neuroanatomy of visuospatial working memory in fragile X syndrome: relation to behavioral and molecular measures. Am J Psychiatry. 2001; 158:1040–1051. [PubMed: 11431225]

Levenga J, de Vrij FM, Buijsen RA, Li T, Nieuwenhuizen IM, Pop A, Oostra BA, Willemsen R. Subregion-specific dendritic spine abnormalities in the hippocampus of Fmr1 KO mice. Neurobiol Learn Mem. 2011; 95:467–472. [PubMed: 21371563]

Liu ZH, Chuang DM, Smith CB. Lithium ameliorates phenotypic deficits in a mouse model of fragile X syndrome. Int J Neuropsychopharmacol. 2011; 14:618–630. [PubMed: 20497624]

Lu Y, Monsivais P, Tempel BL, Rubel EW. Activity-dependent regulation of the potassium channel subunits Kv1.1 and Kv3.1. J Comp Neurol. 2004; 470:93–106. [PubMed: 14755528]

McBride EG, Rubel EW, Wang Y. Afferent regulation of chicken auditory brainstem neurons: rapid changes in phosphorylation of elongation factor 2. J Comp Neurol. 2013; 521:1165–1183. [PubMed: 22987813]

McGlashan TH, Hoffman RE. Schizophrenia as a disorder of developmentally reduced synaptic connectivity. Arch Gen Psychiatry. 2000; 57:637–648. [PubMed: 10891034]

McKinney BC, Grossman AW, Elisseou NM, Greenough WT. Dendritic spine abnormalities in the occipital cortex of C57BL/6 Fmr1 knockout mice. Am J Med Genet B Neuropsychiatr Genet. 2005; 136B:98–102. [PubMed: 15892134]

Miezejeski CM, Heaney G, Belser R, Brown WT, Jenkins EC, Sersen EA. Longer brainstem auditory evoked response latencies of individuals with fragile X syndrome related to sedation. Am J Med Genet. 1997; 74:167–171. [PubMed: 9129717]

Moore JK. Organization of the human superior olivary complex. Microsc Res Tech. 2000; 51:403–412. [PubMed: 11071722]

Murashov AK, Chintalgattu V, Islamov RR, Lever TE, Pak ES, Sierpinski PL, Katwa LC, Van Scott MR. RNAi pathway is functional in peripheral nerve axons. FASEB J. 2007; 21:656–670. [PubMed: 17209129]

Penagarikano O, Mulle JG, Warren ST. The pathophysiology of fragile x syndrome. Annu Rev Genomics Hum Genet. 2007; 8:109–129. [PubMed: 17477822]

Portera-Cailliau C. Which comes first in fragile X syndrome, dendritic spine dysgenesis or defects in circuit plasticity? Neuroscientist. 2012; 18:28–44. [PubMed: 21551076]

Price TJ, Flores CM, Cervero F, Hargreaves KM. The RNA binding and transport proteins staufen and fragile X mental retardation protein are expressed by rat primary afferent neurons and localize to peripheral and central axons. Neuroscience. 2006; 141:2107–2116. [PubMed: 16809002]

Qin M, Entezam A, Usdin K, Huang T, Liu ZH, Hoffman GE, Smith CB. A mouse model of the fragile X premutation: effects on behavior, dendrite morphology, and regional rates of cerebral protein synthesis. Neurobiol Dis. 2011; 42:85–98. [PubMed: 21220020]

Restivo L, Ferrari F, Passino E, Sgobio C, Bock J, Oostra BA, Bagni C, Ammassari-Teule M. Enriched environment promotes behavioral and morphological recovery in a mouse model for the fragile X syndrome. Proc Natl Acad Sci U S A. 2005; 102:11557–11562. [PubMed: 16076950]

Roberts J, Hennon EA, Anderson K, Roush J, Gravel J, Skinner M, Misenheimer J, Reitz P. Auditory brainstem responses in young males with Fragile X syndrome. J Speech Lang Hear Res. 2005; 48:494–500. [PubMed: 15989407]

Roberts TP, Khan SY, Rey M, Monroe JF, Cannon K, Blaskey L, Woldoff S, Qasmieh S, Gandal M, Schmidt GL, Zarnow DM, Levy SE, Edgar JC. MEG detection of delayed auditory evoked responses in autism spectrum disorders: towards an imaging biomarker for autism. Autism Res. 2010; 3:8–18. [PubMed: 20063319]

Roy S, Zhao Y, Allensworth M, Farook MF, LeDoux MS, Reiter LT, Heck DH. Comprehensive motor testing in Fmr1-KO mice exposes temporal defects in oromotor coordination. Behav Neurosci. 2011; 125:962–969. [PubMed: 22004265]

Rubel EW, Parks TN. Organization and development of brain stem auditory nuclei of the chicken: tonotopic organization of n. magnocellularis and n. laminaris. J Comp Neurol. 1975; 164:411–433. [PubMed: 1206127]

Rudelli RD, Brown WT, Wisniewski K, Jenkins EC, Laure-Kamionowska M, Connell F, Wisniewski HM. Adult fragile X syndrome. Clinico-neuropathologic findings. Acta Neuropathol. 1985; 67:289–295. [PubMed: 4050344]

Sanchez JT, Seidl AH, Rubel EW, Barria A. Control of neuronal excitability by NMDA-type glutamate receptors in early developing binaural auditory neurons. J Physiol. 2012; 590:4801–4818. [PubMed: 22826130]

Sanchez JT, Wang Y, Rubel EW, Barria A. Development of glutamatergic synaptic transmission in binaural auditory neurons. J Neurophysiol. 2010; 104:1774–1789. [PubMed: 20668278]

Santoro MR, Bray SM, Warren ST. Molecular mechanisms of fragile X syndrome: a twenty-year perspective. Annu Rev Pathol. 2012; 7:219–245. [PubMed: 22017584]

Schecterson LC, Sanchez JT, Rubel EW, Bothwell M. TrkB downregulation is required for dendrite retraction in developing neurons of chicken nucleus magnocellularis. J Neurosci. 2012; 32:14000–14009. [PubMed: 23035107]

Schrier M, Severijnen LA, Reis S, Rife M, van't Padje S, van Cappellen G, Oostra BA, Willemsen R. Transport kinetics of FMRP containing the I304N mutation of severe fragile X syndrome in neurites of living rat PC12 cells. Exp Neurol. 2004; 189:343–353. [PubMed: 15380484]

Scotto-Lomassese S, Nissant A, Mota T, Néant-Féry M, Oostra BA, Greer CA, Lledo PM, Trembleau A, Caillé I. Fragile X mental retardation protein regulates new neuron differentiation in the adult olfactory bulb. J Neurosci. 2011; 31:2205–2215. [PubMed: 21307257]

Seidl AH, Grothe B. Development of sound localization mechanisms in the mongolian gerbil is shaped by early acoustic experience. J Neurophysiol. 2005; 94:1028–1036. [PubMed: 15829592]

St John JA, et al. Sequencing three crocodilian genomes to illuminate the evolution of archosaurs and amniotes. Genome Biol. 2012; 13:415. [PubMed: 22293439]

Smith ZD. Organization and development of brain stem auditory nuclei of the chicken: dendritic development in N. laminaris. J Comp Neurol. 1981; 203:309–333. [PubMed: 7320232]

Smith DJ, Rubel EW. Organization and development of brain stem auditory nuclei of the chicken: dendritic gradients in nucleus laminaris. J Comp Neurol. 1979; 186:213–239. [PubMed: 447882]

Smith ZD, Gray L, Rubel EW. Afferent influences on brainstem auditory nuclei of the chicken: n. laminaris dendritic length following monaural conductive hearing loss. J Comp Neurol. 1983; 220:199–205. [PubMed: 6315783]

Sorensen SA, Rubel EW. The level and integrity of synaptic input regulates dendrite structure. J Neurosci. 2006; 26:1539–1550. [PubMed: 16452677]

Sorensen SA, Rubel EW. Relative input strength rapidly regulates dendritic structure of chick auditory brainstem neurons. J Comp Neurol. 2011; 519:2838–2851. [PubMed: 21500196]

Strumbos JG, Brown MR, Kronengold J, Polley DB, Kaczmarek LK. Fragile X mental retardation protein is required for rapid experience-dependent regulation of the potassium channel Kv3.1b. J Neurosci. 2010; 30:10263–10271. [PubMed: 20685971]

Teder-Sälejärvi WA, Pierce KL, Courchesne E, Hillyard SA. Auditory spatial localization and attention deficits in autistic adults. Brain Res Cogn Brain Res. 2005; 23:221–234. [PubMed: 15820630]

Thomas CC, Combe CL, Dyar KA, Inglis FM. Modest alterations in patterns of motor neuron dendrite morphology in the Fmr1 knockout mouse model for fragile X. Int J Dev Neurosci. 2008; 26:805–811. [PubMed: 18638539]

Till SM, Wijetunge LS, Seidel VG, Harlow E, Wright AK, Bagni C, Contractor A, Gillingwater TH, Kind PC. Altered maturation of the primary somatosensory cortex in a mouse model of fragile X syndrome. Hum Mol Genet. 2012; 21:2143–2156. [PubMed: 22328088]

Tobia MJ, Woodruff-Pak DS. Delay eyeblink classical conditioning is impaired in Fragile X syndrome. Behav Neurosci. 2009; 123:665–676. [PubMed: 19485573]

Vergne AL, Pritz MB, Mathevon N. Acoustic communication in crocodilians: from behaviour to brain. Biol Rev Camb Philos Soc. 2009; 84:391–411. [PubMed: 19659884]

Wang Y, Cunningham DE, Tempel BL, Rubel EW. Compartment-specific regulation of plasma membrane calcium ATPase type 2 in the chick auditory brainstem. J Comp Neurol. 2009; 514:624–640. [PubMed: 19365819]

Wang Y, Rubel EW. Rapid regulation of microtubule-associated protein 2 in dendrites of nucleus laminaris of the chick following deprivation of afferent activity. Neuroscience. 2008; 154:381–389. [PubMed: 18440716]

Wang Y, Rubel EW. In vivo reversible regulation of dendritic patterning by afferent input in bipolar auditory neurons. J Neurosci. 2012; 32:11495–11504. [PubMed: 22895732]

Wang, Y., Sanchez, JT., Rubel, EW. Nucleus laminaris. In: Shepherd, G., Addona, DD., editors. Handbook of Brain Microcircuits. New York: Oxford University Press; 2010. p. 224-233.

Weibrecht I, Lundin E, Kiflemariam S, Mignardi M, Grundberg I, Larsson C, Koos B, Nilsson M, Söderberg O. In situ detection of individual mRNA molecules and protein complexes or post-translational modifications using padlock probes combined with the in situ proximity ligation assay. Nat Protoc. 2013; 8:355–372. [PubMed: 23348363]

Wisniewski KE, French JH, Fernando S, Brown WT, Jenkins EC, Friedman E, Hill AL, Miezejeski CM. Fragile X syndrome: associated neurological abnormalities and developmental disabilities. Ann Neurol. 1985; 18:665–669. [PubMed: 4083849]

Zangenehpour S, Cornish KM, Chaudhuri A. Whole-brain expression analysis of FMRP in adult monkey and its relationship to cognitive deficits in fragile X syndrome. Brain Res. 2009; 1264:76–84. [PubMed: 19368811]

Zarnescu DC, Shan G, Warren ST, Jin P. Come FLY with us: toward understanding fragile X syndrome. Genes Brain Behav. 2005; 4:385–392. [PubMed: 16098136]

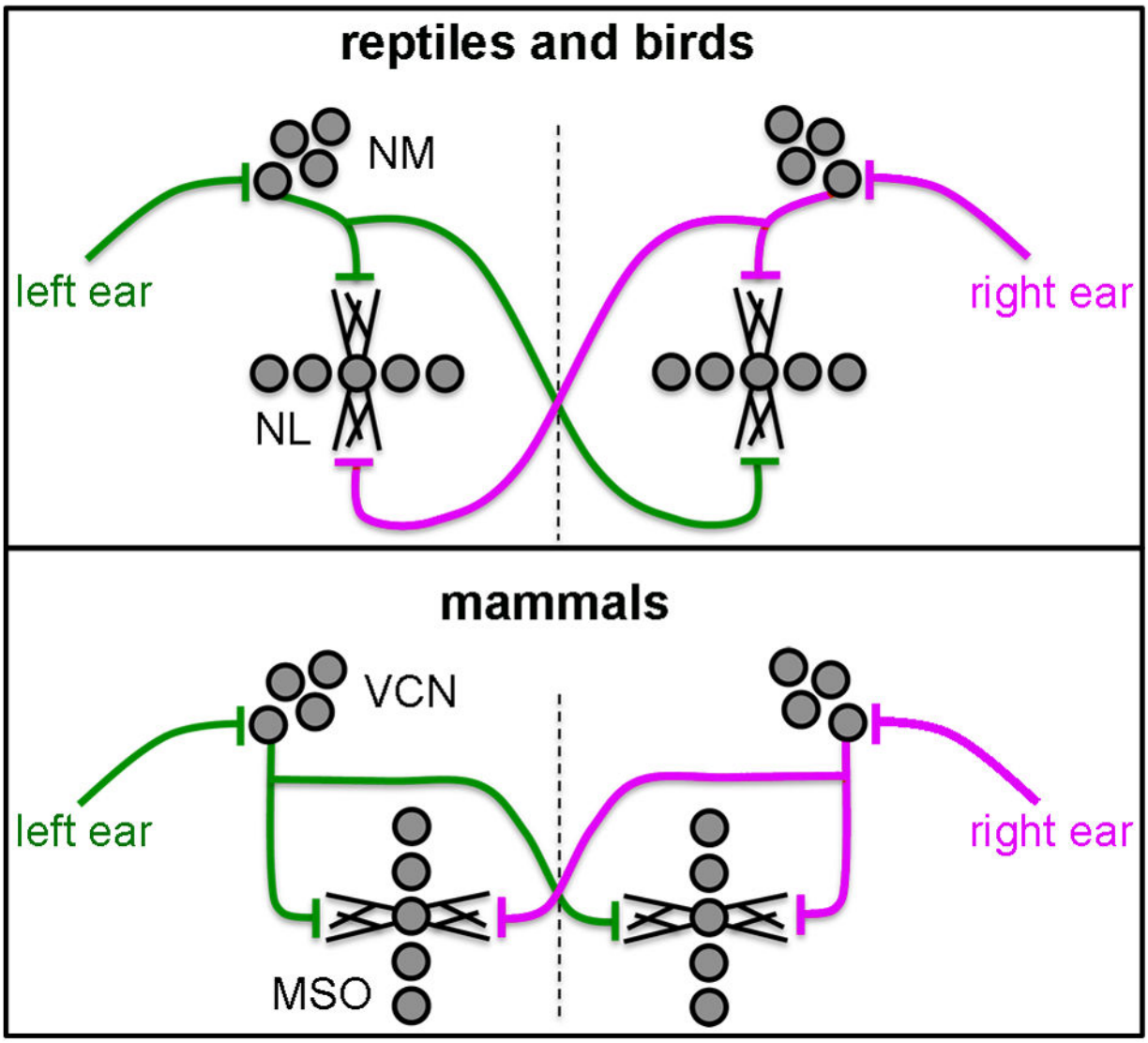

Figure 1.

Schematic drawings of the organization of the binaural circuit in the reptilian, avian, and mammalian auditory brainstem. The reptilian and avian NM and NL are structurally and functionally similar to the mammalian VCN and MSO, respectively. The two dendritic domains of individual bipolar neurons in NL and MSO receive segregated excitatory inputs from the two ears. More specifically, cochlear ganglion cells provide excitatory input to the ipsilateral VCN in mammals and NM in reptiles and birds. Individual VCN and NM neurons project bilaterally to the segregated MSO and NL dendrites, respectively. In mammals, one collateral ends on the lateral dendrites and the cell body of the ipsilateral MSO neurons with the other collateral projecting to the medial dendrite and the cell body of the contralateral MSO. In birds and presumably in reptiles, this pattern is preserved, with NM neurons projecting to the dorsal dendritic domain of the ipsilateral NL and the ventral domain of the contralateral NL. Dashed lines indicate the midline. Dorsal is up. Abbreviations: NM,

nucleus magnocellularis; NL, nucleus laminaris; VCN, ventral cochlear nucleus; MSO, medial superior olive.

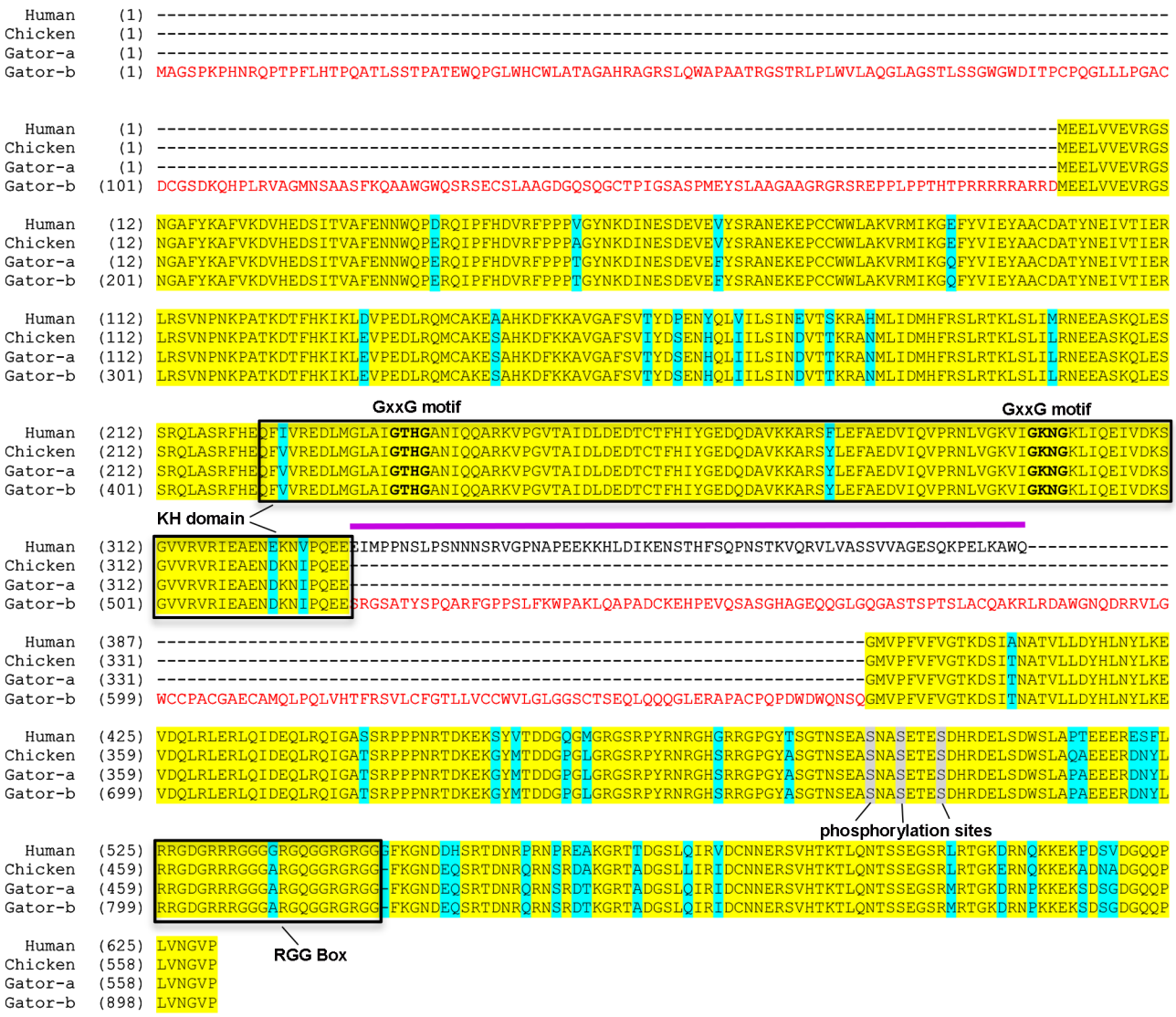

Figure 2.

Amino acid alignment of the alligator, chicken, and human FMRP. Identical and different amino acids across sequences are highlighted in yellow and cyan, respectively. Gator-a is the alligator sequence assembled by screening the alligator genome with the chicken sequence. Gator-b is the alligator sequence predicted by Genscan. Compared to Gator-a, Gator-b contains a long extension at the amino-terminus and a large sequence in the middle of the protein (amino acids in red). The 66-amino-acid gap in the chicken and Gator-a sequences, indicated by a magenta line, corresponds to exon 11 and 12 of the human sequence. KH domain and RGG box are designated by boxes, while phosphorylation sites are highlighted in grey. The GxxG motifs within the KH domain are indicated in bold.

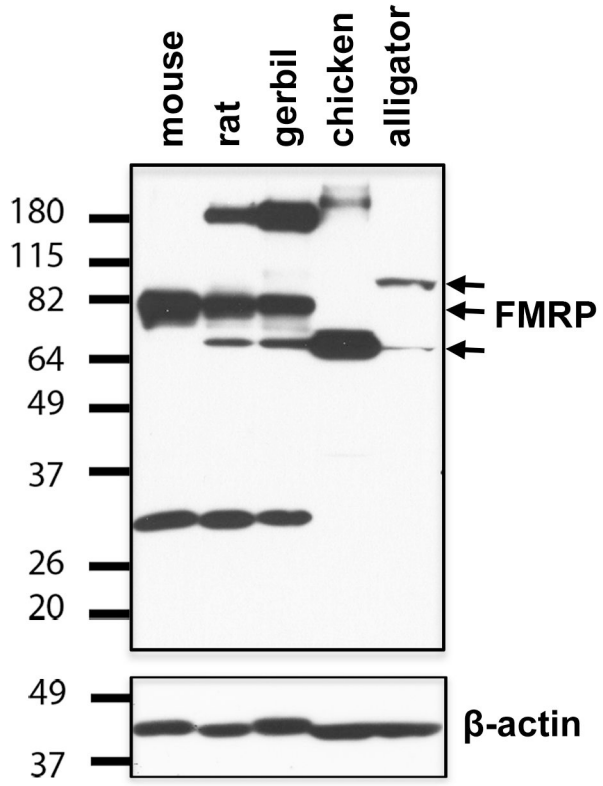

Figure 3.

Western blot assay of anti-FMRP on brain tissues from the mouse, rat, gerbil, chicken, and alligator. Molecular weight standards (left) were used to determine relative sizes of labeled protein bands. Arrows point to the bands of FMRP within predicted molecular weight range. The membrane was stripped and reblotted for β-actin to assess loading. Approximate amount of total protein loaded is 10 μg for the mouse, rat, and gerbil lanes and 30 μg for the chicken and alligator lanes.

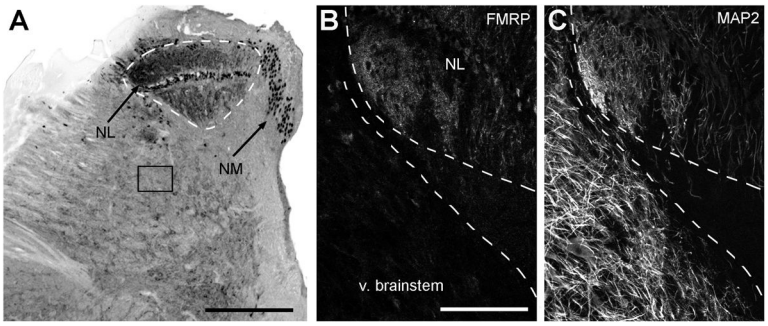

Figure 4.

High intensity of FMRP immunoreactivity in the alligator NL. **A,** Low power image of FMRP immunoreactivity in the caudodorsal brainstem of the alligator. Dorsal is up and medial is right. NM and NL contain dramatically higher levels of FMRP immunoreactivity compared to the majority of other regions in the brainstem. The box indicates the approximate brainstem region used for the quantitative analysis in Fig. 6A. **B–C,** Higher power images of FMRP (B) and MAP2 (C) staining. B and C were taken from a double-labeled section that is adjacent to the section illustrated in A. The intensity of FMRP immunoreactivity in NL is notably higher than that in the adjacent ventral brainstem (v. brainstem) that contains a high level of MAP2-stained dendritic branches. Dashed lines outline the boundary of NL in A and the borders between NL and the ventral brainstem in B–C. See Fig. 5 for closer views. Scale bar = 500 μm in A; 200 μm in B (applies to B–C).

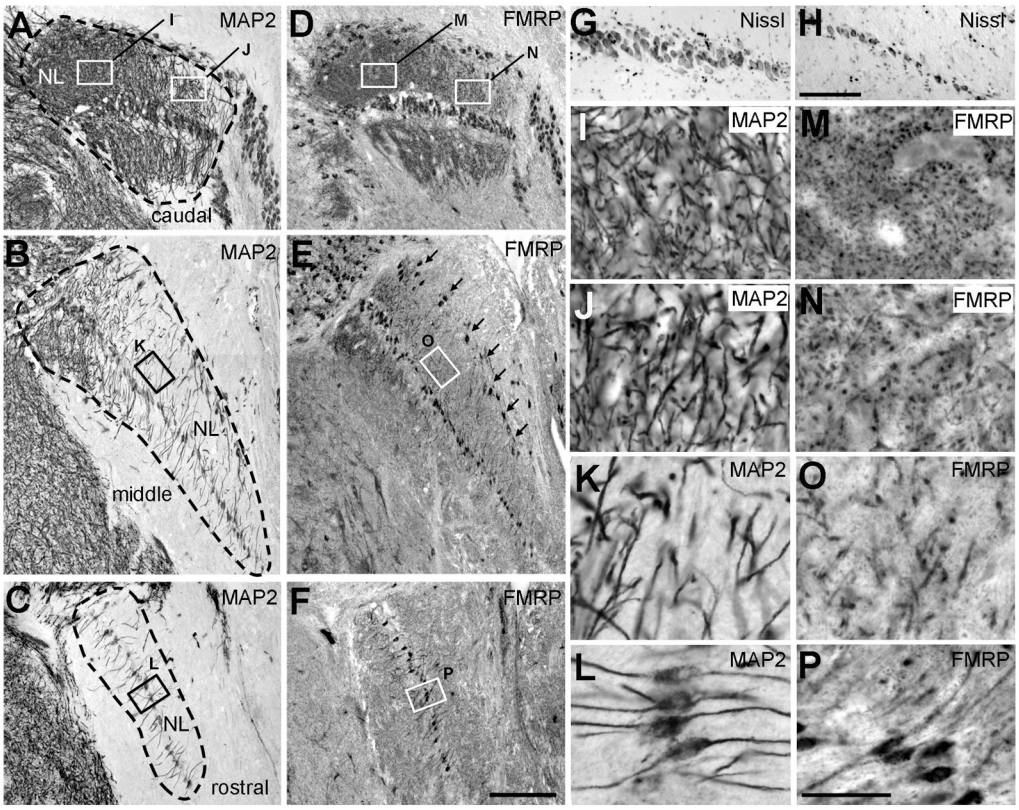

Figure 5.

Dendritic organization and FMRP immunostaining in the alligator NL. **A–C,** Immunostaining for MAP2 in the caudal (A), middle (B) and rostral (C) NL. Dashed lines outline the boundaries of NL. Note the gradient of dendritic extension and branch density along the caudolateral and rostromedial axis of the nucleus. **D–F,** Immunostaining for FMRP in sections adjacent to those in A–C. Arrows in E indicate an array of FMRP-containing neurons along the dorsal edge of the NL. **G–H,** Nissl staining illustrates the multiple layers of cell bodies in the caudolateral NL (G) and the single cell layer in the rostromedial NL (H). **I–J,** Closer views of the boxes in A–C show the gradient of dendritic branch density from caudolateral to rostromedial. **M–P,** Closer views of the boxes in D–F show varying patterns of FMRP staining in the dendritic layers from caudolateral to rostromedial. Dorsal is up and medial is right. Scale bar = 200 μm in F (applies to A–F); 100 μm in H (applies to G–H); 50 μm in P (applies to I–P).

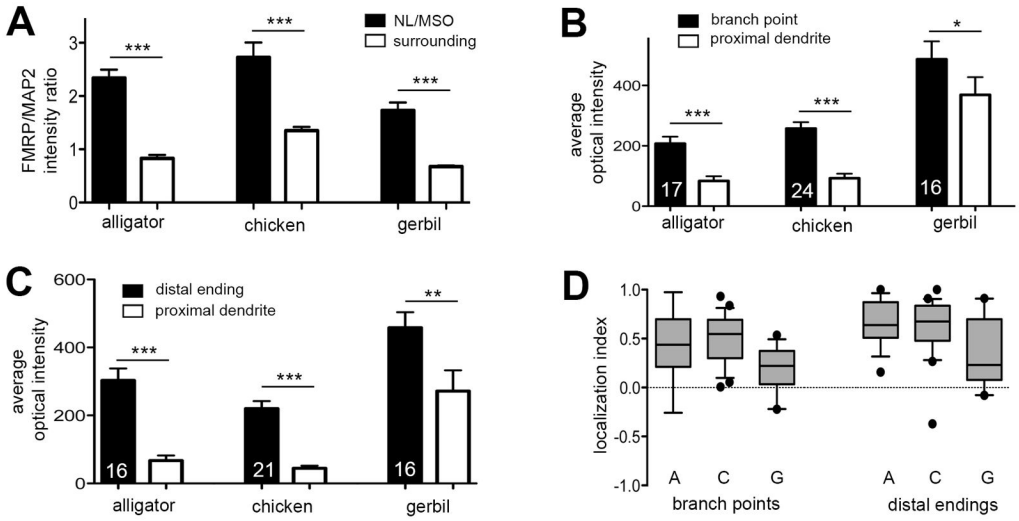

Figure 6.

Quantitative analyses of FMRP immunoreactivity in NL and MSO. **A,** FMRP/MAP2 intensity ratio in NL/MSO dendritic layers (solid) and the surrounding brainstem regions (empty) for each species. Error bars are S.D. *** indicates $p < 0.0001$. **B,** Average optical intensity of FMRP staining at branch points (solid) and the proximal dendritic shafts (empty) of the same branches. Number on each bar indicates the number of sampled branches for each species. Error bars are S.D. * indicates $p < 0.05$. *** indicates $p < 0.0001$. **C,** Average optical intensity of FMRP staining at enlarged distal tips (solid) and the proximal dendritic shafts (empty) of the same branches. Number on each bar indicates the number of sampled terminals for each species. Error bars are S.D. ** indicates $p < 0.001$. *** indicates $p < 0.0001$. **D,** Box-and-Whisker plot of localization index for branch points and enlarged distal tips in each species. The bottom and top of the box are the first and third quartiles, and the band inside the box is the second quartile (the median). Whiskers present 5–95 percentile while outliers are indicated by black dots. Localization index is calculated as the difference in the optical intensity between a branch point (or enlarged distal tip) and its proximal shaft normalized to the sum of the two intensities. A positive localization index indicates a higher level of FMRP in a branch point (or enlarged distal tip) than in the proximal shaft. Abbreviations in D: A, alligator; C, chicken; G, gerbil.

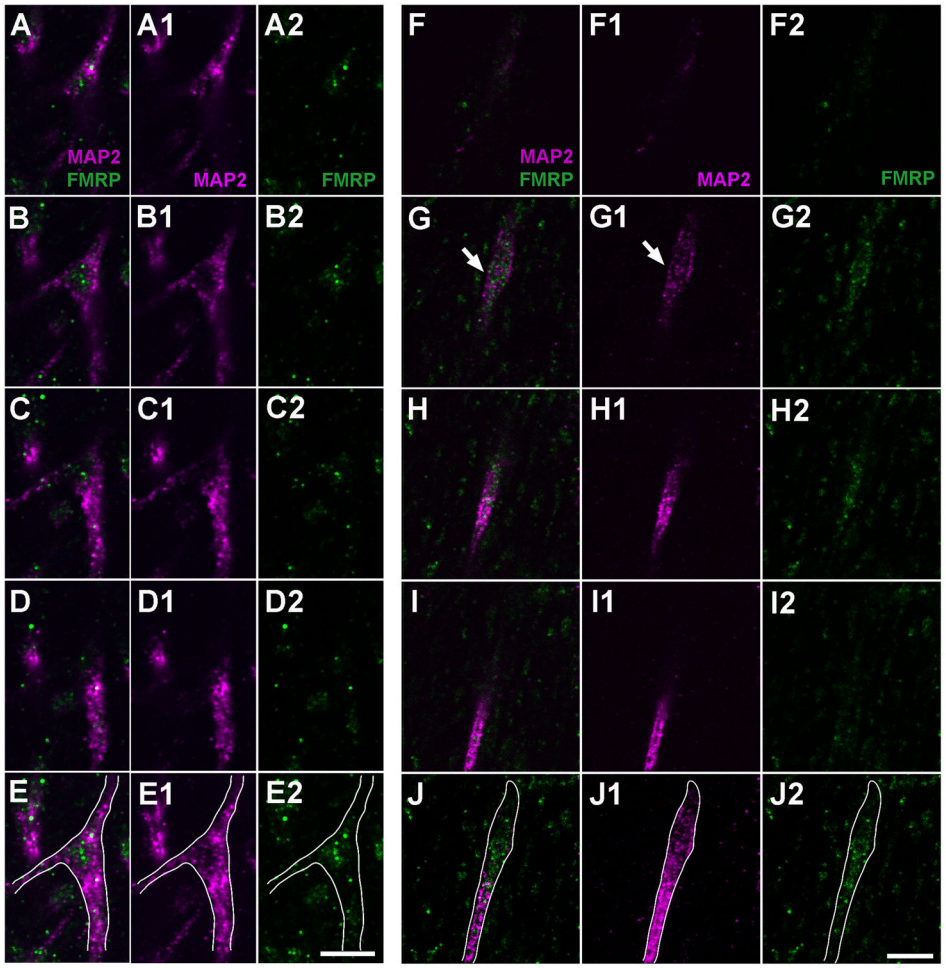

Figure 7.

Subcellular localization of FMRP in NL dendrites of the alligator. **A–E,** FMRP accumulation at a branch point. Note the relatively lower level of MAP2 staining at the branch point. A to D is an image series from different single focus planes while E is the maximum z projection of these images. The first column (A, B, C, D) is the merged images of the second (A1, B1, C1, D1) and third (A2, B2, C2, D2) columns. White lines in E, E1, and E2 outline the dendritic branch. **F–J,** FMRP accumulation at a distal ending. Note the ending is characterized with an enlarged bulge (white arrow) and contains a relatively lower level of MAP2 staining. F to I is an image series from different single focus planes while J is the maximum z projection of these images. The first column (F, G, H, I) is the merged images of the second (F1, G1, H1, I1) and third (F2, G2, H2, I2) columns. White lines in J, J1, and J2 outline the dendritic branch. Scale bar = 5 μm in E2 (applies to A–E2); 5 μm in J2 (applies to F–J2).

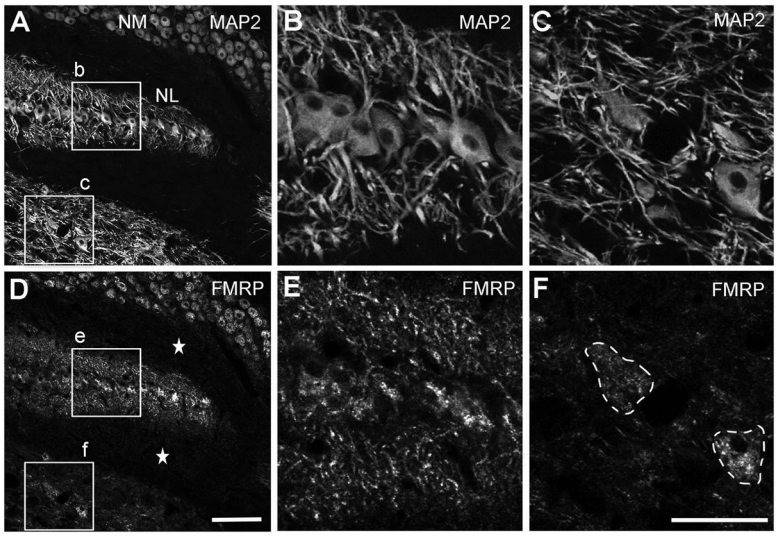

Figure 8.

Low power images of FMRP immunostaining in the chicken NL. **A–C,** Immunostaining for MAP2 in a section containing the caudal NL. B and C are the closer views of the boxes in A. **D–F,** Immunostaining for FMRP taken from the same region of the same section as A–C. E and F are the closer views of the boxes in D. Strong FMRP immunoreactivity is distributed throughout NL in both cell bodies and dendritic layers. FMRP intensity in NL dendritic layers (E) is much higher than the surrounding areas of ventral brainstem (F) which contains a comparable density of dendritic branches assessed by MAP2 staining (B–C). Dashed lines in F outline two stained cell bodies. Dorsal is up and medial is right. Scale bar = 100 μm in D (applies to A and D); 50 μm in F (applies to B–C and E–F).

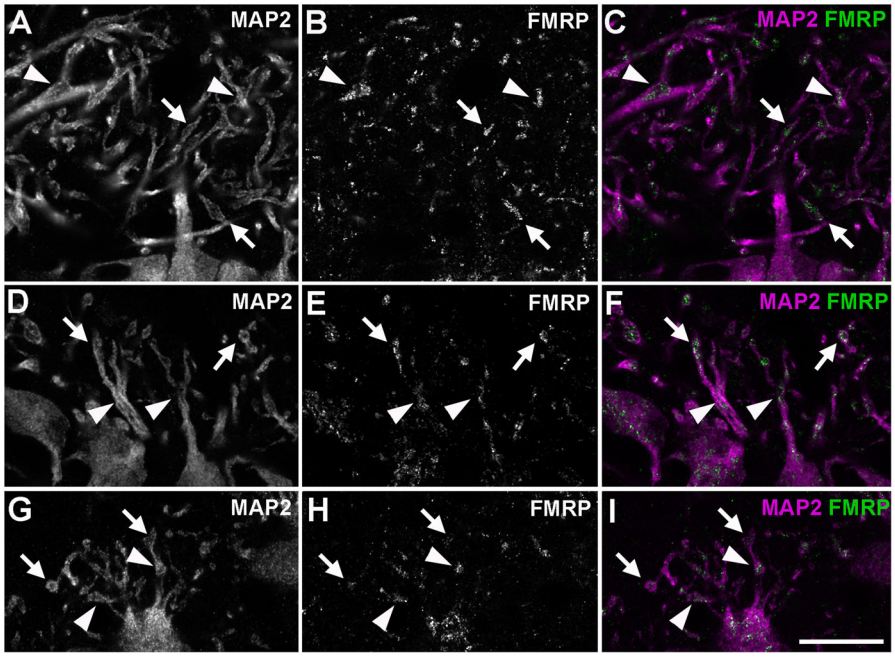

Figure 9.

Dendritic gradient and localization pattern of FMRP immunoreactivity in the chicken NL. Images were taken from the caudal (**A–C**), middle (**D–F**), and rostral (**G–I**) NL. The first (A, D, G) and second (B, E, H) columns are single channels of MAP2 and FMRP immunostaining, respectively, while the most right column (C, F, I) is merged images. Note the gradient of dendritic extension from the somata from caudolateral to rostromedial. The majority of FMRP immunoreactivity in the dendritic layers forms clusters and overlaps with MAP2-stained dendritic branches. Arrowheads and arrows indicate branch points and enlarged distal tips, respectively. Scale bar = 20 μm in I (applies to A–I).

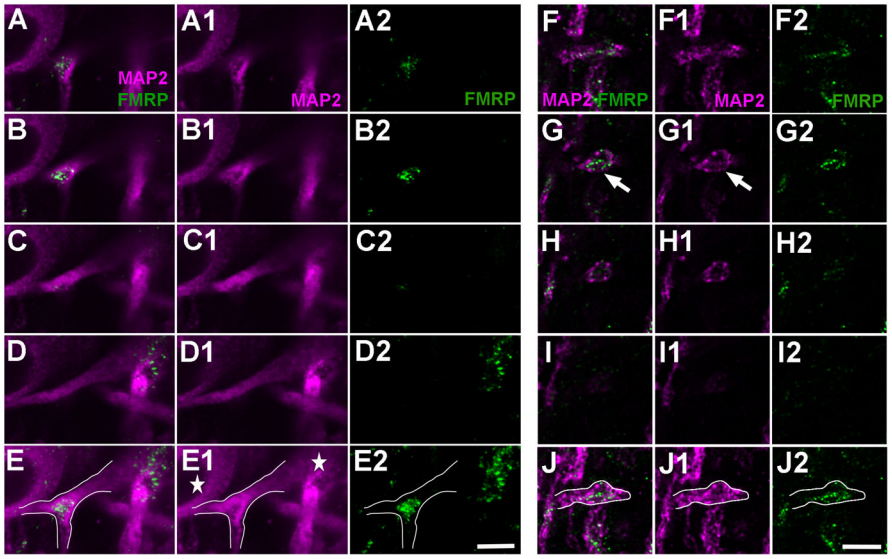

Figure 10.

Subcellular localization of FMRP and MAP2 in NL dendrites of the chicken. **A–E,** FMRP accumulation at a branch point in contrast to the relatively low FMRP intensity in the dendritic shafts of the same and adjacent branches. Note the relatively lower level of MAP2 staining at the branch point. A to D is an image series from different single focus planes while E is the maximum z projection of these images. The first column (A, B, C, D) is the merged images of the second (A1, B1, C1, D1) and third (A2, B2, C2, D2) columns. White lines in E, E1, and E2 outline the dendritic branch. Stars in E1 indicate two cell bodies. **F–J,** FMRP accumulation at a distal ending. Note the ending has an enlarged bulge (white arrow) and contains a relatively lower level of MAP2 staining. F to I is an image series from different single focus planes while J is the maximum z projection of these images. The first column (F, G, H, I) is the merged images of the second (F1, G1, H1, I1) and third (F2, G2, H2, I2) columns. White lines in J, J1, and J2 outline the dendritic branch. Scale bar = 5 μm in E2 (applies to A–E2); 5 μm in J2 (applies to F–J2).

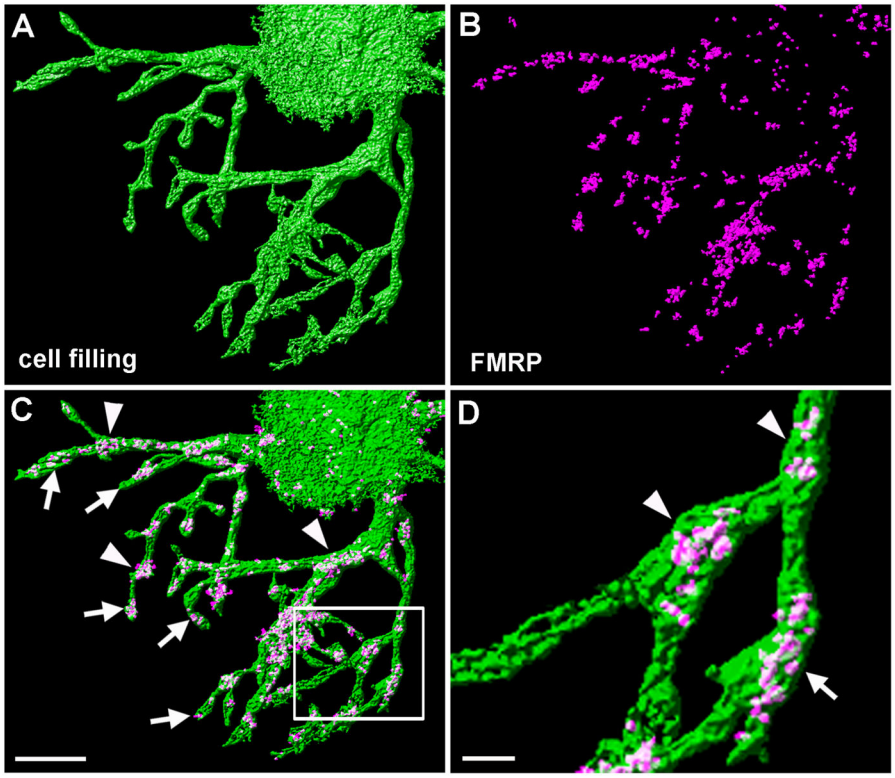

Figure 11.

Dendritic localization of FMRP in individual NL neurons. **A,** Surface rendering of a single NL neuron that was filled with a fluorescent dye. The image here shows the ventral dendritic arborization and a part of the soma (right up corner). **B,** Overlapped FMRP immunoreactivity on dye-filled dendritic branches. Non-overlapping immunoreactivity was removed using the Object Colocalization Analysis function of the Huygens software for visualization. **C,** Merged image of A and B showing strong accumulation of FMRP immunoreactivity in branch points (arrowheads) and enlarged distal tips (arrows). **D,** Closer view of an isolated dendritic branch in the box in C. Scale bar = 10 μm in C (applies to A–C) and 2 μm in D.

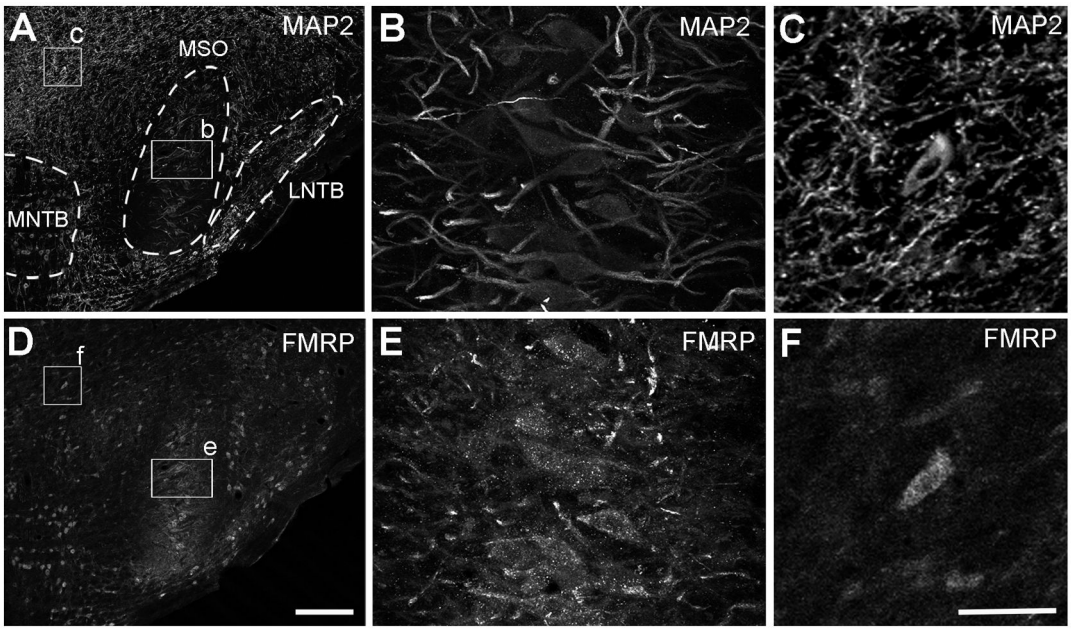

Figure 12.

FMRP immunostaining in the gerbil MSO. **A–C,** Immunostaining for MAP2 in a section containing the rostral MSO. B and C are the closer views of the boxes in A. **D–F,** Immunostaining for FMRP taken from the same region of the same section as A–C. E and F are the closer views of the boxes in D. Strong FMRP immunoreactivity is distributed throughout MSO in both cell bodies and dendritic layers. FMRP intensity in MSO dendritic layers (E) is higher than the adjacent dorsal brainstem (F) which contains a high density of dendritic branches (C). Dashed lines in A outline the boundaries of MSO and other auditory nuclei. Dorsal is up and medial is left. Abbreviations: MSO, medial superior olive; MNTB, medial nucleus of the trapezoid body; LNTB, lateral nucleus of the trapezoid body. Scale bar = 100 μm in D (applies to A and D); 50 μm in F (applies to B–C and E–F).

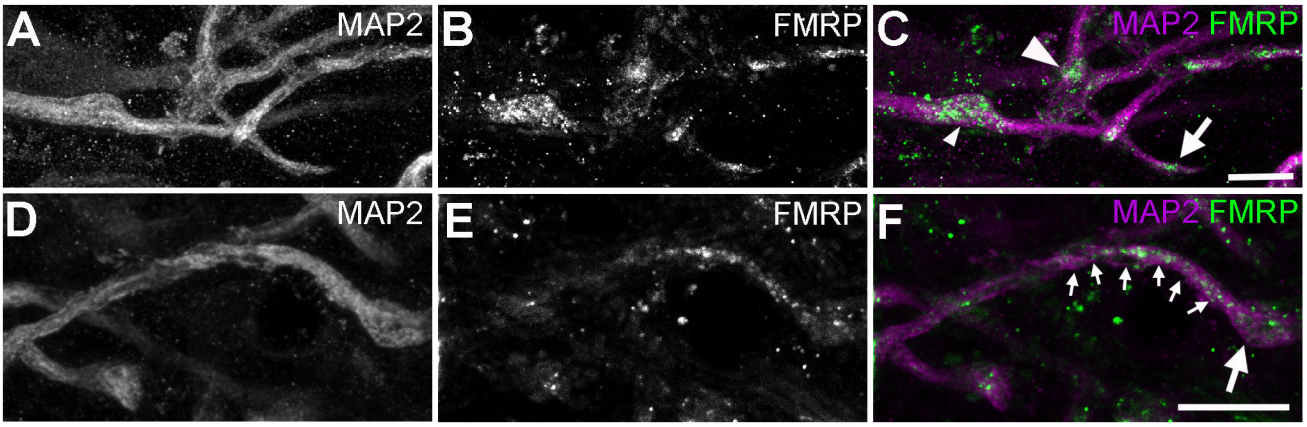

Figure 13.

Dendritic localization of FMRP immunoreactivity in the gerbil MSO. The first (A and D) and second (B and E) columns are single channels of MAP2 and FMRP immunostaining, respectively, while the most right column (C and F) contains merged images. **A–C** illustrate the overlap of FMRP immunoreactivity with MAP2-stained dendritic branches. Dendritic FMRP forms clusters that are distributed along dendritic branches, with high concentrations at branch points (large arrowhead) and enlarged distal tips (arrow). The small arrowheads indicate a dendritic swelling that displays strong staining for FMRP. No branching was detected from the location of this swelling within the section. **D–F** is an example of dendritic branches that contain intense FMRP immunoreactivity both along the main shaft (small arrows) and at the enlarged distal tip (large arrow). Scale bar = 10 μm in C (applies to A–C); 10 μm in F (applies to D–F).

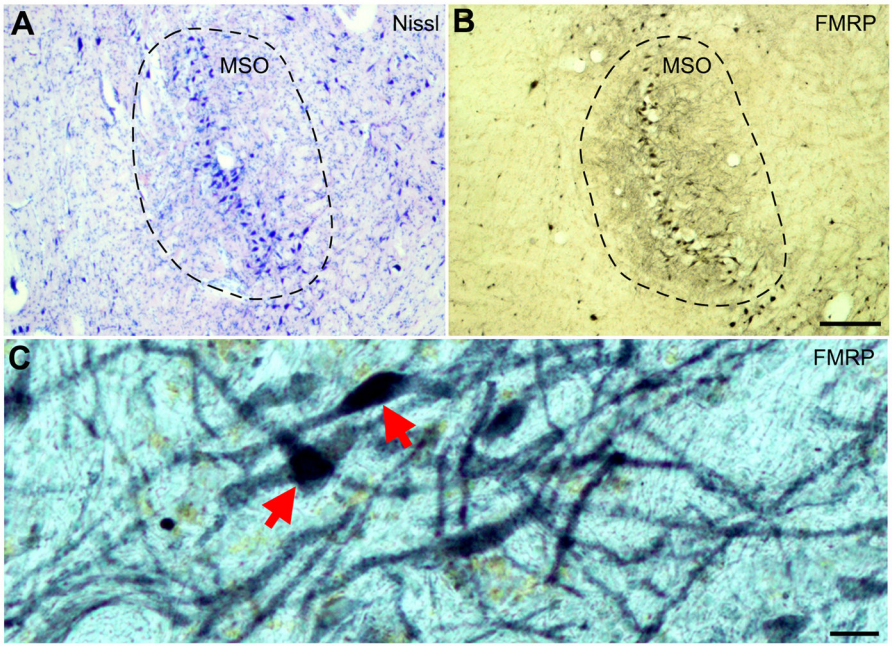

Figure 14.

Nissl stain (A) and FMRP immunoreactivity (B and C) in the human MSO. Dorsal is up and medial is left. Compared to surrounding areas of the brainstem, MSO exhibits a much higher level of FMRP immunoreactivity, particularly in the two dendritic layers. The dashed lines outline the boundaries of the MSO. C is a high power image of FMRP staining in MSO, showing FMRP immunoreactivity in both cell bodies (red arrows) and individual dendritic branches. Scale bar = 100 μm in A (applies to A–B) and 20 μm in C.

Table 1

Primary antibodies and their dilutions used on brainstem tissue of the alligator (a), chicken (c), gerbil (g), rat (r), and human (h).

	Antigen	Host, monoclonal or polyclonal, dilution	Manufacturer, catalog number
FMRP	Synthetic peptide conjugated to KLH derived from within residues 550 to the c-terminus of human FMRP. Contact Abcam for the immunogen sequence.	Rabbit, polyclonal, 1:300 (a), 1:500 (g, r), 1:750 (h), 1:1000 (c)	Abcam PLC (Cambridge, MA), ab17722
MAP2	Bovine brain MAP2 (aa 997–1332)	Mouse, monoclonal, 1:1000 (all species)	EMD Millipore Corporation (Billerica, MA), MAB3418
β-actin	Synthetic peptide derived from within residues 1–100 of human β-actin	Rabbit, polyclonal, 1:1000 (all species)	Abcam PLC, ab8227